Copy No. 10

TTC-1529-R
6 January 1989

Technical Report

TRANSVERSE PUMPING WITH DIODE LASERS

Prepared under:
Contract No. N00014-87-C-2412
INFRARED LASER COUNTERMEASURES

Prepared for:

Mr. John McMahon, Code 6501
Chief Scientist, Optical Sciences Division
NAVAL RESEARCH LABORATORY
4555 Overlook Avenue, SW
Washington, DC 20375-5000

Presented by:

E.B. Treacy
THERMO ELECTRON TECHNOLOGIES CORPORATION
9555 Distribution Avenue
San Diego, California 92121-2305

Copy No. 10

TTC-1529-R
6 January 1989

Technical Report

TRANSVERSE PUMPING WITH DIODE LASERS

Prepared under:
Contract No. N00014-87-C-2412
INFRARED LASER COUNTERMEASURES

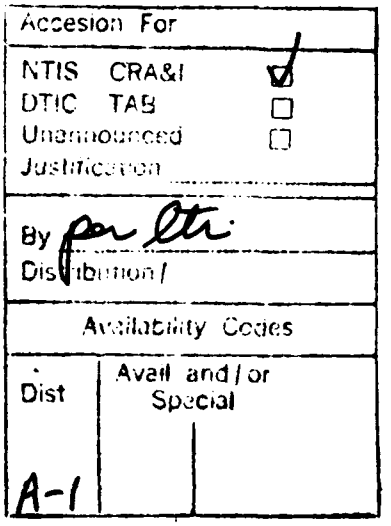

Prepared for:

Mr. John McMahon, Code 6501
Chief Scientist, Optical Sciences Division
NAVAL RESEARCH LABORATORY
4555 Overlook Avenue, SW
Washington, DC 20375-5000

Presented by:

E.B. Treacy
THERMO ELECTRON TECHNOLOGIES CORPORATION
9555 Distribution Avenue
San Diego, California 92121-2305

SUMMARY

The transverse pumping of a cylindrical laser rod such as YAG by a set of diode laser arrays equally spaced in angle around the rod has been analyzed using both geometrical and wave optics. Between the pump sources and the laser rod there may be an arbitrary number of concentric media, transparent to the pump light; and in addition modification of the diode laser radiation patterns will require other optical components. The analysis accommodates both of these complications, even when the optics in front of the diodes do not image point sources to points. It is sufficient to be able to describe the intensity and ray directions in finite apertures concentric with the rod.

One result of the cylindrical geometry is the formation of caustics which have infinite intensity in the geometrical optics approximation; and it is necessary to develop a wave optics theory to predict the intensity in the neighborhood of the caustic edge of the illuminated region inside the laser rod. The wave theory first uses the geometrical optics method to calculate the amplitude and phase just inside the rod's surface, which serves then as an aperture distribution function describing the source of Huygens wavelets in the computation of a diffraction integral. An approximation that assumes constant amplitude and cubic phase distribution along the source surface yields an Airy function description of the caustic intensities that is useful for relating the problem to other known physical phenomena, but overestimates the intensity peak significantly in this case when compared with the results of numerical computation of the integral. Computation

of the diffraction integral is a more convenient method of estimating the peak intensity near the caustic.

A problem with transverse pumping is that if the absorption is small enough to pump the axial region of the rod effectively, a significant fraction of the pump light is transmitted through the rod. This problem can be overcome by reflecting the transmitted light back to the rod. We assume that the reflecting surface is at the same radius as the source images or source apertures. The analysis shows that this measure leads to a high pumping efficiency, defined by the fraction of pump light absorbed in the laser rod. All of our computations of pumping intensity have assumed a Gaussian profile for the source radiation pattern. All pump light outside the limiting rays, which graze the laser rod, is wasted. This is the principal efficiency limiting mechanism according to the present analysis, and this points to the need for mirrors or specially formed lenses near the sources to redirect the radiation.

The analysis has been simplified in many portions, and is presented in a form that makes it easy to program on a computer. The main parts that we did not program are those that would account for longitudinal components in the pump intensity, although we have indicated how this could be done. The two dimensional theory will be adequate for most puposes, specifically in computations that aim at optimizing the design of a laser by maximizing some linear combination of pumping efficiency and deviation from a desired pumping profile. Programs have been written for the IBM PC for computing intensity distributions using both geometrical and wave optics, as well as for investigating numerically some of the relations amongst design parameters.

It is a pleasure to acknowledge the important contributions of O.C. Barr of Pharos Technical Enterprises to the computer programming effort, especially his programming of the diffraction integral developed in the wave optics section of this report, and his persistence in achieving agreement with the results expected from geometrical optics without the use of adjustable multipliers. The key feature of the wave optics, viz. the use of an intermediate surface just inside the surface of the laser rod for defining a source distribution calculated by geometrical optics, was suggested by Rick Kremer.

SECTION 1

TRANSVERSE PUMPING - GEOMETRICAL THEORY

This section treats the transverse pumping of a cylindrical laser rod by diode lasers. The aim is to develop appropriate mathematical formulae to calculate the pump energy distribution in the rod, determine what factors influence the uniformity and efficiency of pump energy deposition, and provide some logical basis for the choice of dimensions, number of arrays on the circle, etc. The simplest approximation is to treat the problem in two dimensions (transverse to the rod axis) and this is done first; but the problem is really three-dimensional, and the relevant equations are developed for this case also.

The geometry.

Figure 1 shows a section of the arrangement of diode arrays pumping a rod. The arrays are equally spaced on the circle. Each array has an associated antenna pattern. A phased array would have a two-lobe pattern, and the arrays would probably be arranged so that the lobe separation is in a direction perpendicular to the figure. Each array may have a lens in front of it. The lenses have three effects: additional attentuation due to surface reflections, transformation of the antenna pattern, and replacement of array positions by image positions. The lens arrangement may produce real or virtual images. Figure 1 is still good. The antenna patterns and array positions are simply those of the images. All formulae developed initially are for the two-dimensional approximation, i.e. all rays are assumed to lie in the plane of the figure.

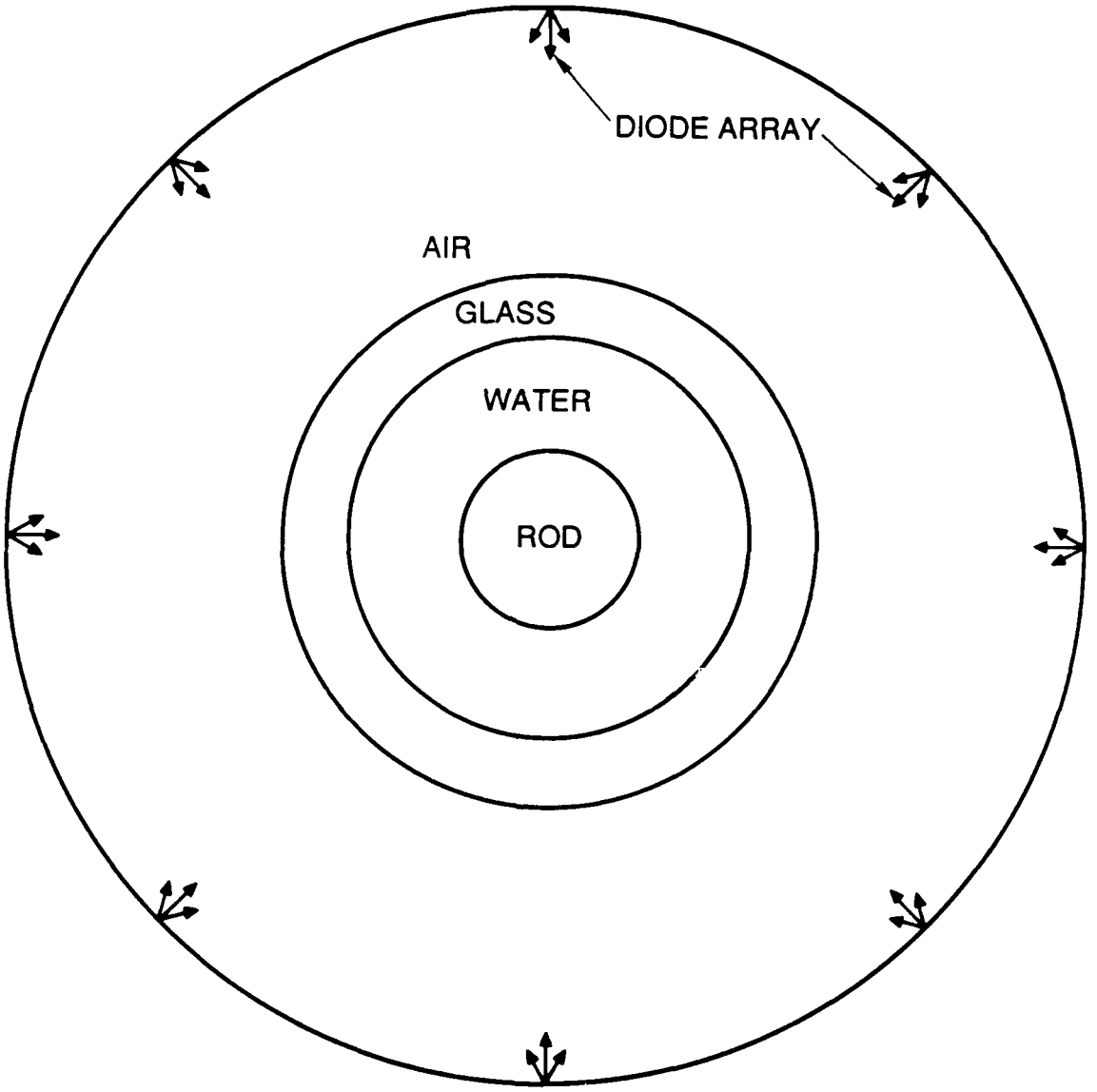

88-7500

Figure 1. Typical geometrical arrangement of diode arrays around a laser rod surrounded by cooling fluid and jacket. The theory is good for any number of concentric media.

Snell's law.

In two-dimensional coordinates (r,θ) *, when the index n is dependent only on r, Snell's law is*

$$n\ r\ \sin\beta = \text{const.}$$

where β *is the angle between the ray and the radius. A point inside the laser rod is denoted by* (a,α)*, and is referred to as the field point. Figure 2 shows how the field point is illuminated by a ray at angle* ϕ *from the array located at* $(R,0)$ *. Concentric media with radii* $r_1, r_2, \ldots r_M$ *and refractive indices* $n_1, n_2, \ldots n_M$ *are shown, with the ray having angles of incidence and refraction* β'_j *and* β_j *at the point* (r_j,θ_j)*. The coordinates* (r_o,θ_o) *and* (r_M,θ_M) *are to be identified with* (a,α) *and* (R,Φ_M) *respectively when the index j takes on its extreme values 0 and M. The angle* Θ *is the position of the diode laser array, and will be denoted by* Θ_i *where i = 1, 2, ...N for N arrays. The angle* ϕ *at which a ray leaves the diode array is identified with* β_M*; and finally, we also use n interchangeably with* n_M*. The closest approach of the ray to the center of the rod is denoted by the distance p. Snell's law applied to Figure 2 gives:*

$$\begin{aligned} n_1 p &= n\ R\ \sin\phi \\ &= n_j r_j\ \sin\beta_j \\ &= n_{j+1}\ r_j\ \sin\beta'_j \end{aligned} \qquad (1)$$

These relations give the various angles in terms of ϕ *. In general, a ray will cut the circle of radius a at two points:* (a,α_1) *and* (a,α_2)*, as shown above in Figure 3. Identifying the ray* ϕ *that goes through the field point* (a,α) *involves expressing* α_1

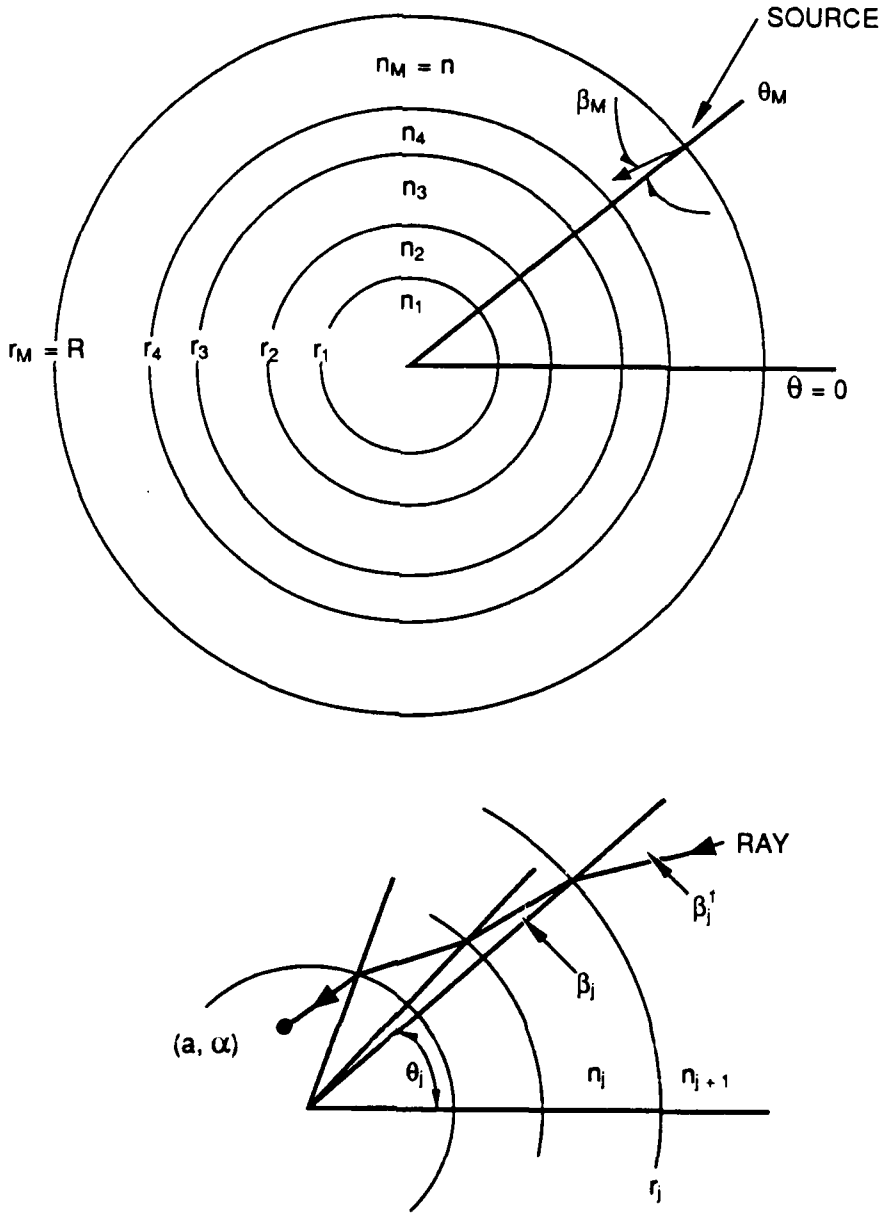

C88-8948

Figure 2. Two-dimensional ray tracing from the sources at (r_M, θ_M) *(also denoted by* (R, Θ)*)* to the field point (r_o, θ_o) *(also denoted by* (a_1, α)*).* The angles of incidence and refraction at the interfaces are β_j' *and* β_j respectively at radius r_j. The special value β_M is also denoted by ϕ.

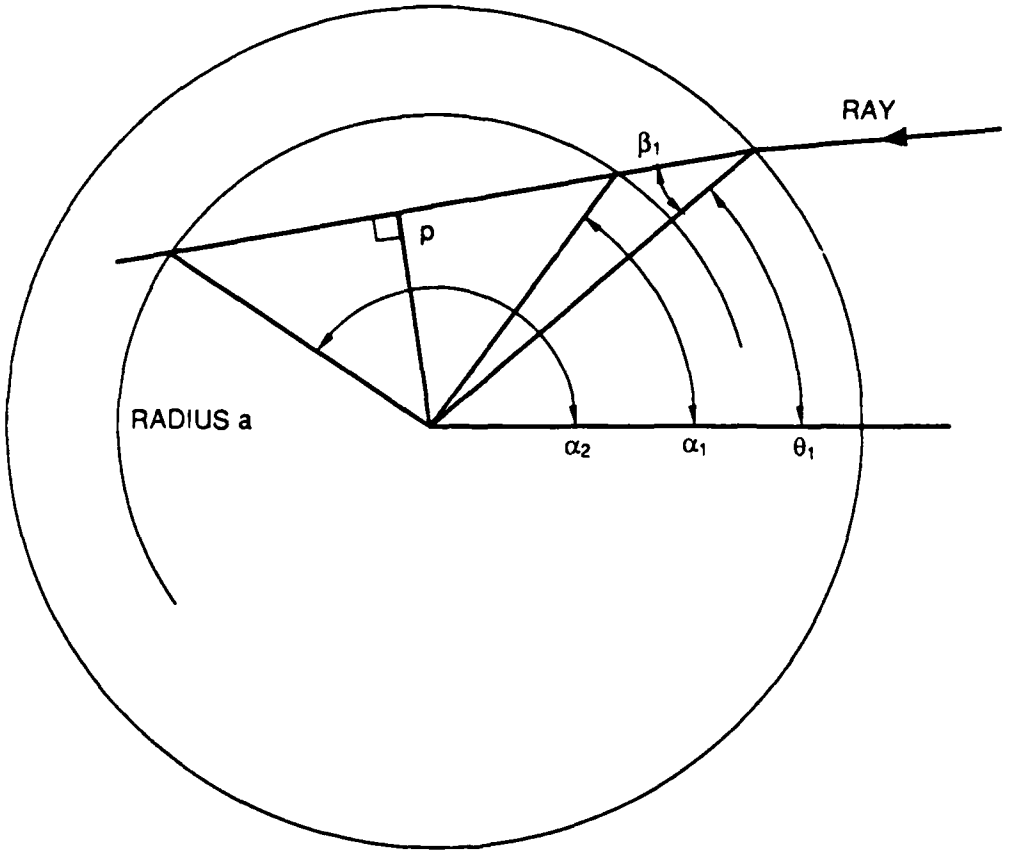

C88-8949

Figure 3. Illustration of how the ray intersects the circle of radius a at two points with polar angles of α_1 *and* α_2.

and α_2 in terms of ϕ . The following relations between the β'_j, β'_j and θ_j :

$$\beta'_{j-1} - \beta_j = \theta_{j-1} - \theta_j \qquad (2)$$

which can be summed over j to give

$$\theta_o - \theta_M = \sum_{j=1}^{M} (\beta'_{j-1} - \beta_j) \qquad (3)$$

where β'_o is seen to be $\sin^{-1}(p/a)$, which by Equation 1 is the same as $\sin^{-1}(\frac{nR}{n_1 a} \sin\phi)$. Note also from Figure 2 that

$$\alpha_2 = \alpha_1 + 2\cos^{-1}(p/a) \qquad (4)$$

Combining Equations 1, 3 and 4 gives:

$$\alpha_1 = \theta_M + \sum_{j=1}^{M} \{\sin^{-1}(\frac{nR}{n_j r_{j-1}} \sin\phi) - \sin^{-1}(\frac{nR}{n_j r_j} \sin\phi)\} \qquad (5a)$$

and

$$\alpha_2 = \alpha_1 + \pi - 2\sin^{-1}(\frac{nR}{n_1 a} \cos\phi) \qquad (5b)$$

Notice that the last term in Eq. 5a reduces (at $j = M$) to ϕ .

As ϕ increases, β'_1 eventually becomes $\pi/2$ which determines the limiting ray beyond which no light enters the rod. From Equation 1, this condition is expressed as

$$\phi_m = \sin^{-1}\left(\frac{n_2 r_1}{nR}\right) \qquad (6a)$$

and the corresponding distance p is

$$p_m = \frac{n\,R}{n_1}\sin\phi_m = \frac{n_2 r_1}{n_1} \qquad (6b)$$

assuming that n_1 is greater than n_2. Light emitted at angles exceeding ϕ_m at the diode array is wasted and this is one reason for considering the use of lenses. (In the present analysis, a Gaussian distribution $\exp - (\phi/\phi_e)^2$ has been assumed.) A lens at a distance u from the point source (section through diode array) produces an image at v from the lens so that the antenna pattern is narrowed by the factor u/v while R increases by -(u + v). (v is positive for a real image.) The focal length and position of the lens would be specified so as to place the image at the desired R and make ϕ_e equal to the desired value.

Equations 1 - 5 above are the basic ray tracing relations in two dimensions. Eq. 5 can be used to find the polar angle α at which a given ray from the source intersects the circle r = a inside the rod. The number of intersections is 2, 1 or 0 depending on whether a is greater or smaller than p_m.

Figure 4 is a plot of Eqs. 5 for a specific concentric geometry chosen for purposes of illustration. Here ϕ_m is 6.07 degrees, for the critical ray. Curves are drawn for six separate values of radius a, with α_1 and α_2 being the lower and upper branches respectively. The branches are separate when a is greater than $(n_2/n_1)r_1$ and form a single curve for smaller values. Curve 4 has a equal to $(n_2/n_1)r_1$ which corresponds to the case in which the critical ray is tangential to the circle. The remaining curves from left to right have a/r_1 equal to 0.2, 0.4, 0.6, 0.8, 1.0 respectively. The curvature of

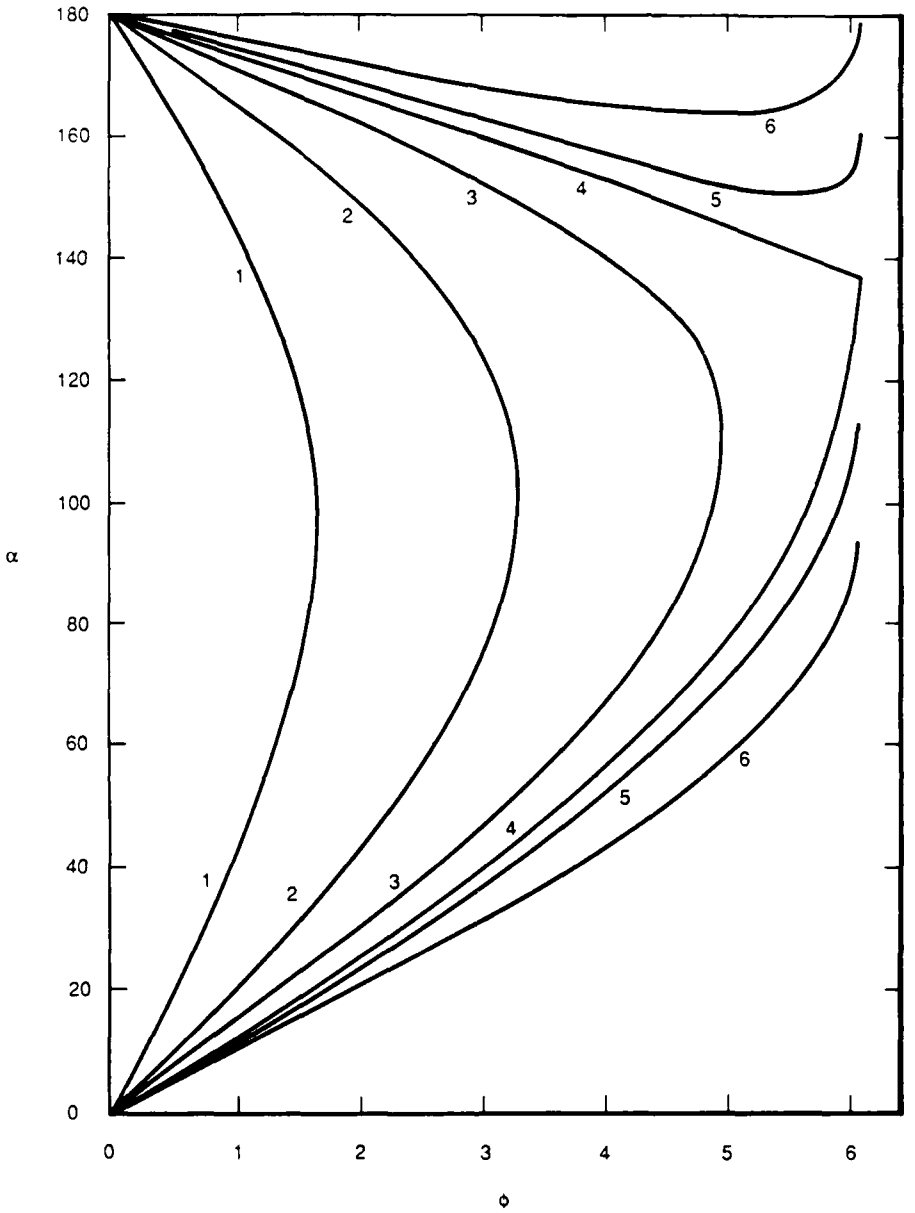

88-8950

Figure 4. Plot of $\alpha_{1,2}$ versus ϕ (both in degrees) for various values of the radius a.

the upper branch (α_2) changes sign as a function of the parameter a on going through the critical value associated with Curve 4, which has a bearing on the use of Newton's method for solving Eq. 5b for ϕ when the coordinates (a,α_2) are specified.

Another point worth noting is the minimum in α_2 when a is greater than $(n_2/n_1)r_1$ (Curves 5 and 6). The minimum makes $\alpha_2(\phi)$ stationary, corresonding to a convergence of rays through the point in question. Such stationary points lie on a caustic that extends from $a = (n_2/n_1)r_1$ to $a = r_1$. By symmetry there are two caustics associated with the pump source at Θ_i, corresponding to positive and negative ϕ. The caustics have anomalously high intensity, and are treated in some detail later in this report. Conventional ray tracing computational techniques that estimate intensities by counting the density of rays tend to miss the anomalous intensities of the caustics.

Equations 5a and 5b are of the form $\alpha \equiv \alpha(\phi)$ where α stands for $\alpha_{1,2}$ and $\alpha(\phi)$ is the right hand side of the respective equations. Finding ϕ for a given point (a,α) is equivalent to solving the equation

$$\alpha(\phi) - \alpha = 0 \; . \qquad (7)$$

This then identifies the ray ϕ_i through the point (a,α) from the source located at θ_{Mi}(or Θ_i for short). . It is necessary to decide which of the two functional forms, 5a or 5b, is the appropriate one to use, corresponding to the first or second intersection of the ray with the circle of radius a. Computationally this is handled by generating a table of $\alpha_{1,2}(\phi)$ and seeing where the target value α lies in relation to the tablulated values. If Newton's method is used, the n-th approximation $\phi_{(n)}$ generates the (n+1)-th by

$$\phi_{(n+1)} = \phi_{(n)} - (\alpha_{1,2}(\phi_{(n)}) - \alpha)/\dot{\alpha}_{1,2}(\phi_n)$$

where $\dot{\alpha}$ stands for the derivative $d\alpha/d\phi$, which is given by

$$d\alpha_1/d\phi = nR\cos\phi \sum_{j=1}^{M} \{(n_j^2 r_{j-1}^2 - n^2R^2 \sin^2\phi)^{-\frac{1}{2}} - (n_j^2 r_j^2 - n^2R^2 \sin^2\phi)^{-\frac{1}{2}} \} \tag{8a}$$

$$d\alpha_2/d\phi = d\alpha_1/d\phi - 2nR\cos\phi(n_1^2a^2 - n^2R^2 \sin^2\phi)^{-\frac{1}{2}} \tag{8b}$$

The Pump Intensity. ***(Single Pass)***

In the two-dimensional approximation the intensity at the field point (a,α) due to one diode or one array is estimated as follows. The antenna pattern at the source is written $dW/d\phi$. (The source is the diode array, or its image.) At the field point, consider a line element dw at right angles to the ray, through which pass all the rays within the source angle element $d\phi$. The power radiated towards this line is $(dW//d\phi)d\phi$ and the intensity at the field point is $(dW/d\phi)(d\phi/dw)$, multiplied by a factor that accounts for propagation losses. The line element length is

$$dw = \left|(a^2 - p^2)^{\frac{1}{2}}\, d\alpha\right| \tag{9}$$

so that the intensity is

$$I(a,\alpha) = \Sigma_i \frac{T_i \dfrac{dW}{d\phi(i)}}{\left|(a^2 - p_i^2)^{\frac{1}{2}} \dfrac{d\alpha}{d\phi(i)}\right|} \tag{10}$$

where all sources on the circle are accounted for in the summation over i. The attenuation factors T_i account for reflection losses at the boundaries, and absorption in the laser rod:

$$T_i = \exp(-\sigma s_{1,2}) \; T(\beta_1) \; T(\beta_2) \; T(\beta_3) \; . \; . \; . \; T(\beta_{M-1}) \qquad (11)$$

where
$$T(\beta_1) = 1 - \frac{\tan^2(\beta_1' - \beta_1)}{\tan^2(\beta_1' + \beta_1)} \qquad (12)$$

for P-polarization of the electric field. For S-polarization tangents are replaced by sines, and this is the more usual case for diode laser arrays. σ is the absorption coefficient in the pump band of the laser rod, and s is the length of the ray from the rod boundary to the field point, given by

$$s_{1,2}^2 = (a^2 - p^2) + (r_1^2 - p^2) \mp 2 \, (a^2 - p^2)^{\frac{1}{2}} \, (r_1^2 - p^2)^{\frac{1}{2}} \qquad (13)$$

The quantities on the right side of Equation 10 are all functions of the respective variables $\phi(i)$. The angles β and β' are all expressed as inverse sine functions of a multiplier times sin $\phi(i)$ as in Equation 5a. Finally, $d\alpha/d\phi(i)$ is given by Equation 8. Computation of the pumping intensity at the field point thus comprises solving the $\phi(i)$ in Equation 7 and substituting values into Eq. 10.

Some Limiting Cases.

When a equals p_i in the denominator of Equation 10 the square root factor becomes zero and the quantity $\dot{\alpha}$ is infinity. However, it is readily shown that the denominator remains finite:

$$\left| \lim_{p \to a} \{(a^2 - p^2)^{\frac{1}{2}} \, d\alpha/d\phi(i)\} \right| = (n/n_1) \, R \cos \phi(i) \qquad (14)$$

At the center of the rod (a=0) the denominator simplifies to (nR/n_1) *because* $\phi(i)$ *is zero. Both numerator and denominator simplify when* $\phi(i)$ *is zero which occurs for* α *equal to* θ *or to* $(\theta + \pi)$ *. In this case the transmission formula becomes*

$$T(\phi = 0) = e^{-\sigma(r_1 \mp a)} \prod_{j-1}^{M-1} \{1-(n_j - n_{j+1})^2/(n_j + n_{j+1})^2\}$$

$$= e^{-\sigma(r_1 \mp a)} \prod_{j=1}^{M-1} t_j \qquad (15)$$

whereas the denominator in Equation 10 reduces to

$$\left|(a^2 - p^2)^{\frac{1}{2}} \, d\alpha/d\phi\right|_{\phi=0} = \left| a \mp R(n/n_1) + a \, R \, n \left\{ \sum_{j=1}^{M-1} \left(\frac{1}{n_j} - \frac{1}{n_{j+1}}\right) \frac{1}{r_j} \right\} \right| \qquad (16)$$

Note that Eq. 15 defines the quantities t_j*. At a=0 we get the same quantity* (nR/n_1) *obtained earlier for the denominator and use Equation 15 for the numerator. In particular the intensity on the axis of the rod is*

$$I(axis) = (n_1/nR) \, N \, T_i(0,0)(dW/d\phi)_{\phi=0} \qquad (17)$$

for N sources, where $T_i(0,0)$ *is the expression in Eq. 15 evaluated at* $a = 0$ *i.e. the absorption factor is* $e^{-\sigma r_1}$ *. For a single source (N=1) the last few equations lead to a simple formula for the intensity any-*

where along the diameter aligned with the source. For example at $(r_1,0)$, which is just inside the laser rod on the central ray, we have

$$I(axis)/I(r_1,0) = (n_1 r_1/2h)\, e^{-\sigma r_1} \qquad (18a)$$

where

$$(1/2h) = \sum_{j=2}^{M} (1/n_j)(1/r_{j-1} - 1/r_j) \; . \qquad (18b)$$

It can be shown that h is the coefficient of the quadratic term in θ_1 in the expression for the optical path length S_2 from the source to the edge of the rod (r_1,θ_1) , i.e.

$$S_2(\theta_1) = S_2(0) + h\theta_1^2 + O(\theta_1^4) \qquad (19)$$

which determines the curvature of the wavefront incident on the laser rod surface.

Normalization of the Pump Intensity.

In the two-dimensional geometry the antenna pattern from the pump source is considered to be a function of the single variable ϕ . The quantity $dW/d\phi$ in Eq. 10 needs to be expressed in terms of P/L, the power per unit length radiated by the diode array of length L. It is clear that

$$P/L = \int (dW/d\phi)\, d\phi \qquad (20)$$

and it is instructive to assume that the pattern $dW/d\phi$ is a Gaussian function:

$$dW/d\phi = (dW/d\phi)_{\phi=0} \exp -(\phi/\phi_e)^2 \qquad (21)$$

Then the integral in Eq. 20 is $(dW/d\phi)_{\phi=0}\ \phi_e\ \pi^{\frac{1}{2}}$ which evaluates $(dW/d\phi)_{\phi=0}$ so that Eq. 21 becomes

$$dW/d\phi = (P/L)(1/\phi_e\ \pi^{\frac{1}{2}}) \exp -(\phi/\phi_e)^2 \qquad (22)$$

Thus it is easy to substitute for $dW/d\phi$ in Eq. 10, or for $(dW/d\phi)_{\phi=0}$ in Eq. 17 to calculate the intensity.

In some of our computational illustrations the diode laser antenna pattern has been normalized simply to $\exp -(\phi/\phi_e)^2$. When this is done the power radiated per unit length of diode array is $\phi_e\pi^{\frac{1}{2}}$, and the computed intensities in the rod refer to this source strength. For unit source strength (1 watt/cm) the computed intensities would need to be divided by $\phi_e\pi^{\frac{1}{2}}$. These cases will be identified in the figure captions where they occur. It is more convenient to build the normalization factor $1/(\phi_e\pi^{\frac{1}{2}})$ right into the computer program as we have done more recently, so that the results give intensity (watts/cm^2) corresponding to unit source strength (1 watt/cm). With N source arrays, the pump light near the axis is arrriving in N different directions. The units of intensity that we use (watts/cm^2) are still valid because the total transition probably for pumping an atom or ion is the sum over the individual contributions irrespective of their directions.

A Computational Example.

The following example is used to illustrate the use of the theory so far presented. Consider a YAG rod of radius 0.3175 cm. (This is a quarter inch diameter.) The surface of the rod is assumed to be

smooth so that the laws of refraction apply. The rod is surrounded by cooling water enclosed in a glass jacket. Five pumping sources are equally spaced on a circle of radius 4 cm. We are interested in the pump intensity distribution inside the rod, which is assumed to have an attenuation factor of 3, so that the total attenuation along a diameter is exp - (0.3175 x 3) = 0.39 . Light that passes through the rod is wasted in this computational example. The pumping sources are assumed to have ϕ_e *equal to 6.46 degrees. (The source strength is 0.1998, which is* $\phi_e \pi^{\frac{1}{2}}$ *.) These sources would most likely be the virtual images of real diode arrays situated on a smaller radius than 4 cm, radiating into a positive lens, because the arrays normally have a wider antenna pattern. The pump light is assumed to have S-polarization of its electric field i.e. polarized along the direction of the array. The fraction of pump light radiating at angles less than* ϕ_{max} *is given by the Error Function erf (0.940). (This number is 0.816.) Light at larger angles is wasted, as it cannot enter the laser rod.*

At any fixed radius a the intensity has five equal cycles in the 360 degrees, and shows symmetry about any diameter through a source. Therefore we need to tabulate only within the range 0 to 36 degrees.

In the computations the refractive indices assumed are 1.823, 1.333, 1.5 and 1 for the media. The geometry is shown in Figure 5.

Figure 6 shows intensity versus angle at radial steps of $r_1/10$. *Notice that from the center* $(a/r_1 = 0)$ *out to* $a = 0.7r_1$ *there is very little angular variation in intensity. At radii exceeding* $p_m(0.7312\ r_1)$ *the effects of caustics show up. (See lowest three curves in Fig. 6.) There is a smooth drop of intensity with increasing radius along radii bisecting or passing through the sources because in these special cases no caustics cross these radii.*

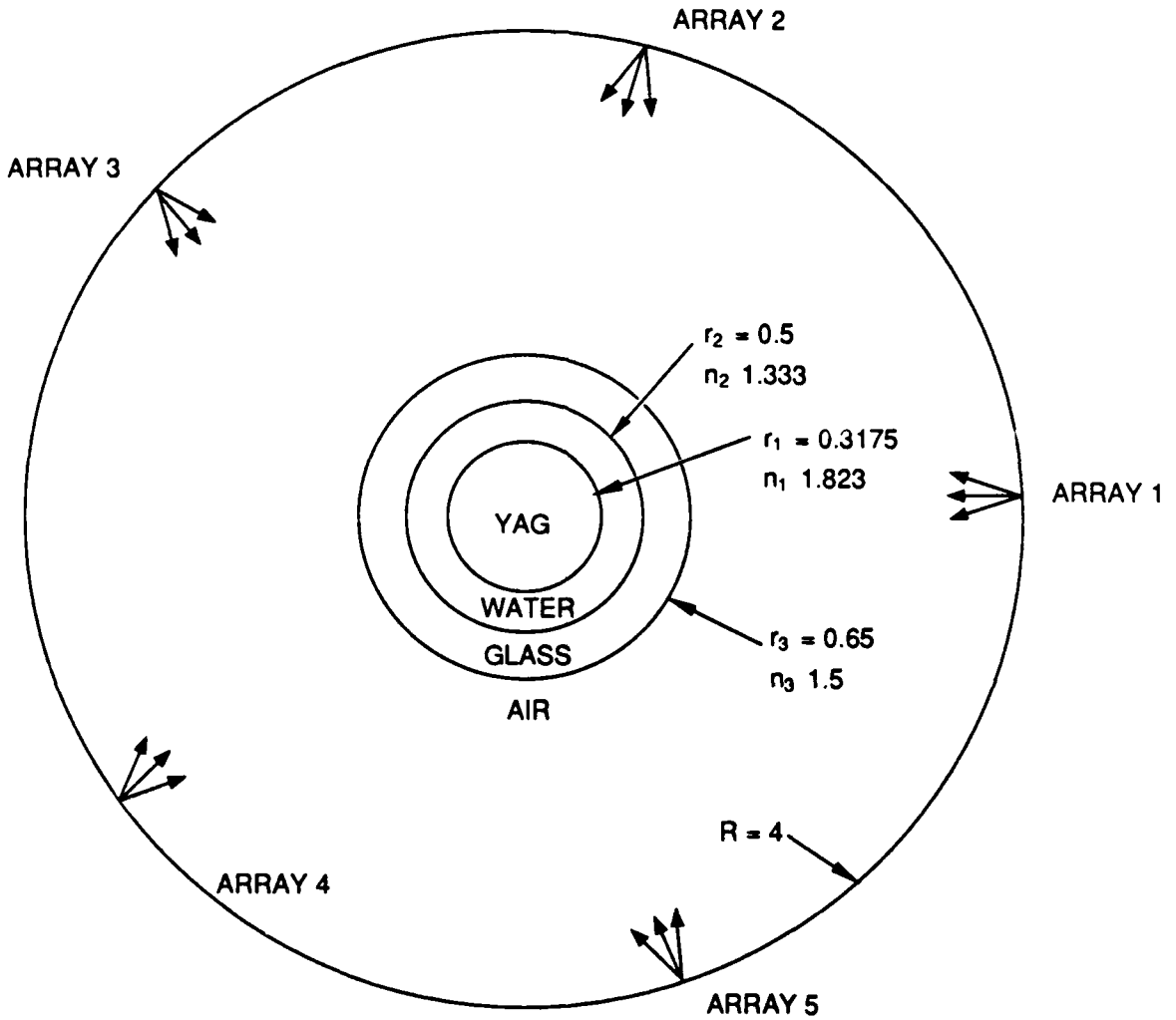

C88-8951

Figure 5. This shows the geometry used for the computations shown in Figure 6. The array positions are those of the images made by the focussing lenses, if any are used.

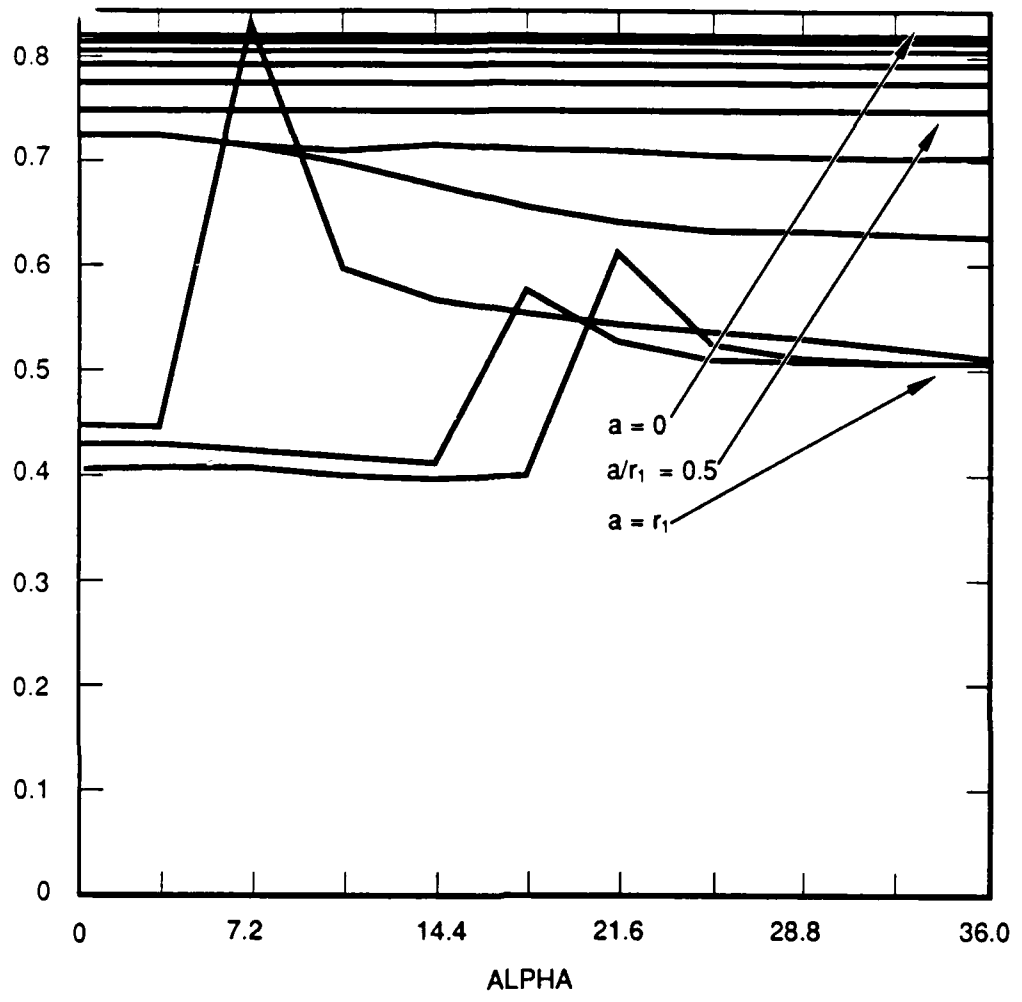

C88-8952

Figure 6. Intensity versus angle at various radii (normalized to rod radius r_1) for the geometry shown in Figure 5. The antenna width ϕ_e is 6.46 degrees (0.1127 radian), so that the power radiated from each source is 0.1998 watt per centimeter.

General Considerations.

Irrespective of the distance R (locating the point source) there are two segments unilluminated as illustrated in Figure 7. These segments are bounded by arcs of angle $(\alpha_2 - \alpha_1)$ *evaluated at* $a = r_1$, *i.e.*

$$Arc = \pi - 2 \sin^{-1}(n_2/n_1)$$

Likewise the perpendicular distance

$$p_m = n_2 r_1 / n_1$$

is invariant. What varies with R is the angle τ_m *that* p_m *makes with the central ray. This angle is given by the following equation.*

$$\begin{aligned} \tau_m &= \tfrac{1}{2} (\alpha_1 + \alpha_2)_{MAX} \\ &= \theta + \pi + \sum_{j=3}^{M} \sin^{-1}(n_2 r_1 / n_j r_{j-1}) \\ &\quad - \sum_{j=1}^{M} \sin^{-1}(n_2 r_1 / n_j r_j) \end{aligned} \qquad (23)$$

The quantity nR should be chosen to set ϕ_m *at the most desirable value with respect to the antenna pattern of the diode array. If the angular width of the pattern is excessive a lens might be used to alter it. Another consideration is the variation in pump intensity due to the focussing property of the optical arrangement. In terms of x measured along the central ray as illustrated in Figure 7, the intensity obtained from Equations 10, 15 and 16 is*

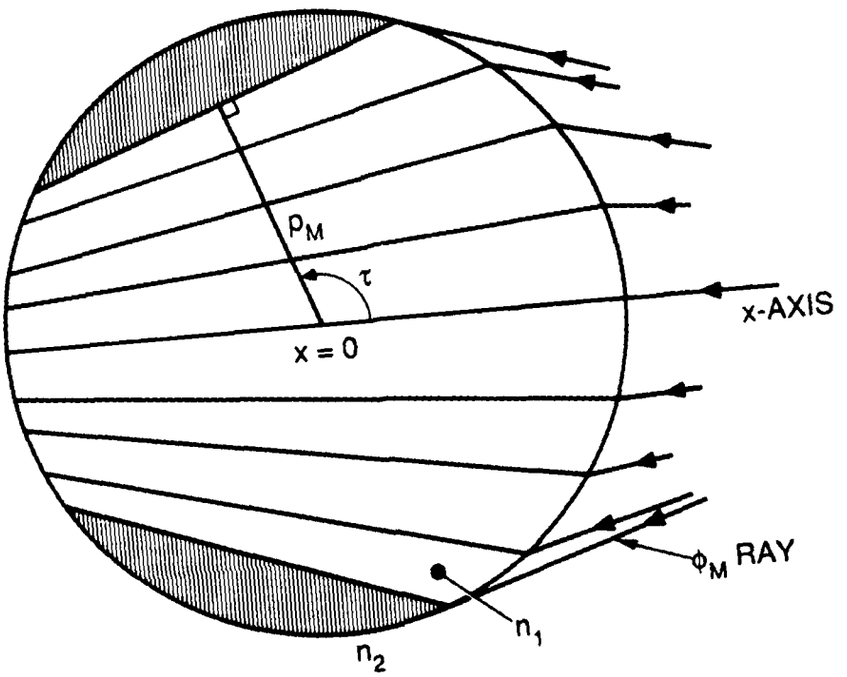

88-7501

Figure 7. Illustration of the unilluminated segments, shown shaded. As shown later, the left ends of the shaded regions are bounded by curved caustics that start at the mid-points of the chords, i.e. at the points $(p_m, \pm \tau_m)$.

$$I(x) = \frac{1}{R}\left(\frac{n_1}{n}\right) e^{-\alpha_1 l} \prod_{j=3}^{M-1} t_j \, J(x)$$

where the t-functions are those in braces in Equation 15, and J(x) is given by

$$J(x) = e^{\sigma x} / |(1 + bx) \qquad (24a)$$

where

$$b = \frac{1}{r_1} - \frac{n_1}{2h} \qquad (24b)$$

with h defined in Eq. 18b. (Equation 24 applies on the x-axis only.) b may be made positive or negative by appropriate choice of parameters. It is readily shown that dJ/dx is zero and d^2J/dx^2 is minimum when b equals σ , which thus gives the condition for the most uniform pump distribution along the central ray near the center of the rod, from a single array. (This is not a really significant result, though.)

The following is an approach to the problem of seeking the most uniform pump distribution around the axis of the rod for multiple diode arrays. The transverse variation is best approximated near the center by looking at the values along the locus p = a, where from Equations 10 and 14 we have for a single array.

$$I\left(\phi = \sin^{-1}\frac{n_1 p}{nR}\right) = \frac{\prod_j T(\beta_j)\,\frac{dW}{d\phi}}{\frac{n}{n_1} R \cos\phi} \qquad (25)$$

wherein p will be replaced by x. (Here we assume that the source lies on the y-axis, so that p lies approximately along x for small p.) This expression is an even function of x that will be expanded as far as quadratic terms. The various factors give:

$$e^{-\sigma(r_1^2 - p^2)^{\frac{1}{2}}} = e^{-\sigma r_1}(1 + \tfrac{1}{2}\frac{\sigma}{r_1}x^2)$$

$$\frac{dW}{d\phi}\ (\text{if Gaussian}) = 1 - \left(\frac{n_1}{n\,R\phi_e}\right)^2 x^2$$

$$\frac{1}{\cos\phi} = 1 + \tfrac{1}{2}\left(\frac{n_1}{n\,R}\right)^2 x^2$$

Neglecting the variation in the T(β) functions, the result is

$$I(x)/I(o) = 1 + x^2\{\tfrac{1}{2}\frac{\sigma}{r_1} - \frac{n_1}{nR})^2(\frac{1}{\phi_e^2} - \tfrac{1}{2})\} + O(x)^4$$

$$= 1 + \{\tfrac{1}{2}\frac{\sigma}{r_1} - \left(\frac{n_1}{n\,R\,\phi_e}\right)^2\}\,x^2 \qquad (26)$$

where we assume $\phi_e^2 << 2$.

Consider four equally spaced pump beams (two opposing pairs at right angles). Along one of the axes the variation from one pair of beams goes like

$$|J(x)| + |J(-x)| = 2(\cosh \sigma x - bx \sinh \sigma x)/(1 - b^2 x^2)$$

$$= 2 + \{(\sigma - b)^2 + b^2\} x^2 + O(x^4) \qquad (27)$$

if bx is less than unity, while the contribution of the other two is twice the right side of Equation 26 above. The coefficient of x^2 *vanishes, giving the condition for most uniform intensity variation around the axis, when*

$$(\sigma - b)^2 + b^2 + \frac{\sigma}{r_1} = 2\left(\frac{n_1}{n R \phi_e}\right)^2$$

or equivalently:

$$\phi_e = \frac{\sqrt{2}\ \left(\frac{n_1}{nR}\right)}{\left[(\sigma - b)^2 + b^2 + \frac{\sigma}{r_1}\right]^{\frac{1}{2}}} \qquad (28)$$

where b = b(R) as in Equations (24b) and (18b). Once the laser rod and water jacket sizes are chosen as in Figure 2 for example, Equation 28 can be represented by a set of curves in the (ϕ_e, R) *plane with parameter* σ *. Figure 8 shows such a set for a YAG rod, water and glass water jacket of dimensions indicated in the figure.*

Although the conditions for uniform pumping have been derived for four beams, obviously the same conditions would apply for eight or twelve. We can assume that they would be accurate for any other number above four.

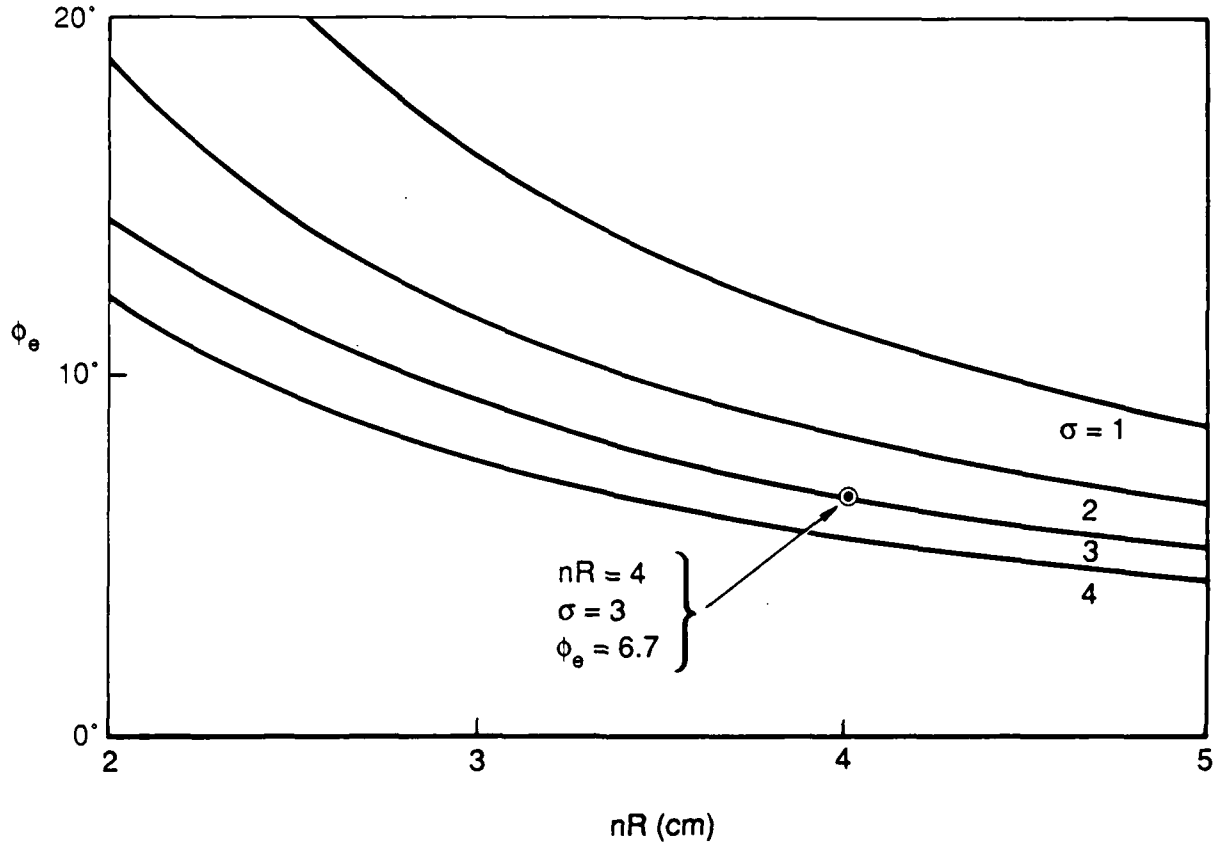

88-7503

Figure 8. Antenna width in formula $exp\ [-(\phi/\phi_e)^2]$ that gives flattest pump distribution of axis of rod versus diode radial distance for various assumed pump band coefficients σ in the expression $exp\ [-\sigma\ x]$. The geometry in shown in Figure 5.

The motivation for seeking a uniform energy deposition over the cross section of the rod is that it comprises a first step in understanding the more complete problem that optimizes distribution of thermally induced strain, population inversion, and temperatures.

Multipass Analysis.

The results shown in Figure 6 show that the pumping intensity can be made fairly uniform over about one half the cross section area, but there is a pumping efficiency penalty in that a large fraction of the pump light is transmitted through the rod. The efficiency can be increased by increasing the absorption coefficient σ *. Another approach is to reflect the transmitted light.*

Suppose that the pump arrays are separated by sections of a cylindrical mirror of radius R. Then a ray at angle ϕ *, after passing through the laser rod strikes the mirror at angle of incidence equal to* ϕ *, because as shown in Figure 9, the ray path is symmetrical about the perpendicular p. After reflection the ray will leave the mirror surface at an angle* ϕ *. All rays that pass through the rod will make a set of rays displaced an angle* 2τ *from one set to the next, where*

$$\tau = \tfrac{1}{2}(\alpha_1 + \alpha_2) \qquad (23)$$

(τ *is negative when* ϕ' *is positive. See Figure 9.) The N arrays lay down a pattern of 2N rays belonging to angles* $\pm\,\phi$ *on the first pass. These rays lie within the ring bounded by radii* $p(\phi)$ *and* r_1 *. After one reflection of each, there are now an additional 2N rays within the same ring; and each successive reflection produces a further 2N rays. Light at a smaller angle* ϕ' *similarly produces a pattern of rays bounded by* $p(\phi')$ *and* r_1 *, overlapping the first ring that we considered. The illumination within the circle* $a(\phi < \phi_M)$ *has been found by computation*

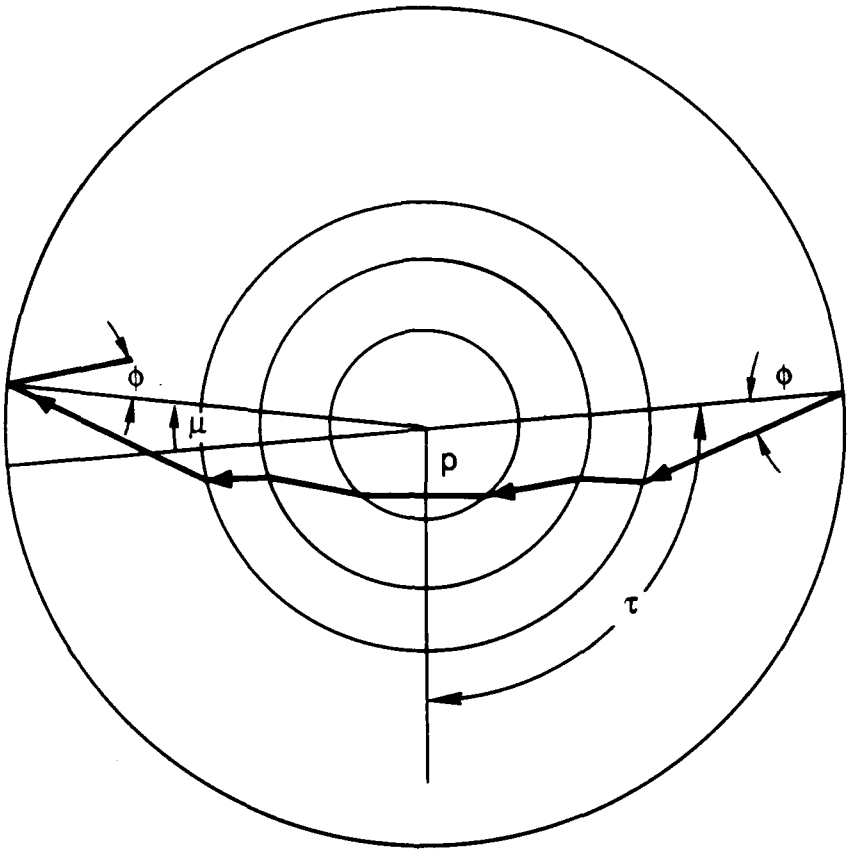

88-7508

Figure 9. In one pass through the system a ray from the source at angle ϕ advances in position on the circle of radius R by 2τ. A plot of 2τ *against* ϕ for a typical case is shown in Figure 11.

to be essentially independent of angle α of the (a,α) , for five or more arrays. The addition of interlaced rays in the same domain produced by the reflections from the cylindrical mirror would not be expected to essentially change this circular symmetry. We assume then, without mathematical proof, that the intensity in the rod will be at least as symmetrical as for the single pass and that the contribution from all rays at any angle ϕ will be equivalent to the single pass contribution from an antenna intensity $dW'/d\phi$ related to $dW/d\phi$ by

$$\frac{dW'}{d\phi} = \frac{dW}{d\phi}\left[1 + \rho(\phi) + \rho^2(\phi) + \rho^3(\phi) + \ldots\right]$$

$$= \frac{dW}{d\phi}/[1 - \rho(\phi)] \qquad (30)$$

where $$\rho(\phi) = \prod_j T^2(\beta_j)\, e^{-2\sigma\left[r_1^2 - \frac{n^2R^2}{n_1^2}\sin^2\phi\right]^{\frac{1}{2}}} G \qquad (31)$$

Here the $T(\beta)$ are the transmission factors given in Equation 12, the exponential factor accounts for single pass absorption in the rod, and G is the reflection coefficient of gold (0.974). The radial distribution for the multipass case is thus estimated by modifying the antenna pattern as in Equation 30, then doing the single pass computation.

Using Equations 30 and 31 we have calculated the radial distributions shown in Figure 10, where the diode arrays are at R = 4 cm, and $dW/d\phi$ is chosen to be Gaussian with ϕ_e equal to 6.7 degress. With the absorption coefficient σ equal to 3 the parameters are set to the point X in Figure 8 which predicts a uniform pumping near the axis. The calculated distribution in Figure 10 suports this prediction

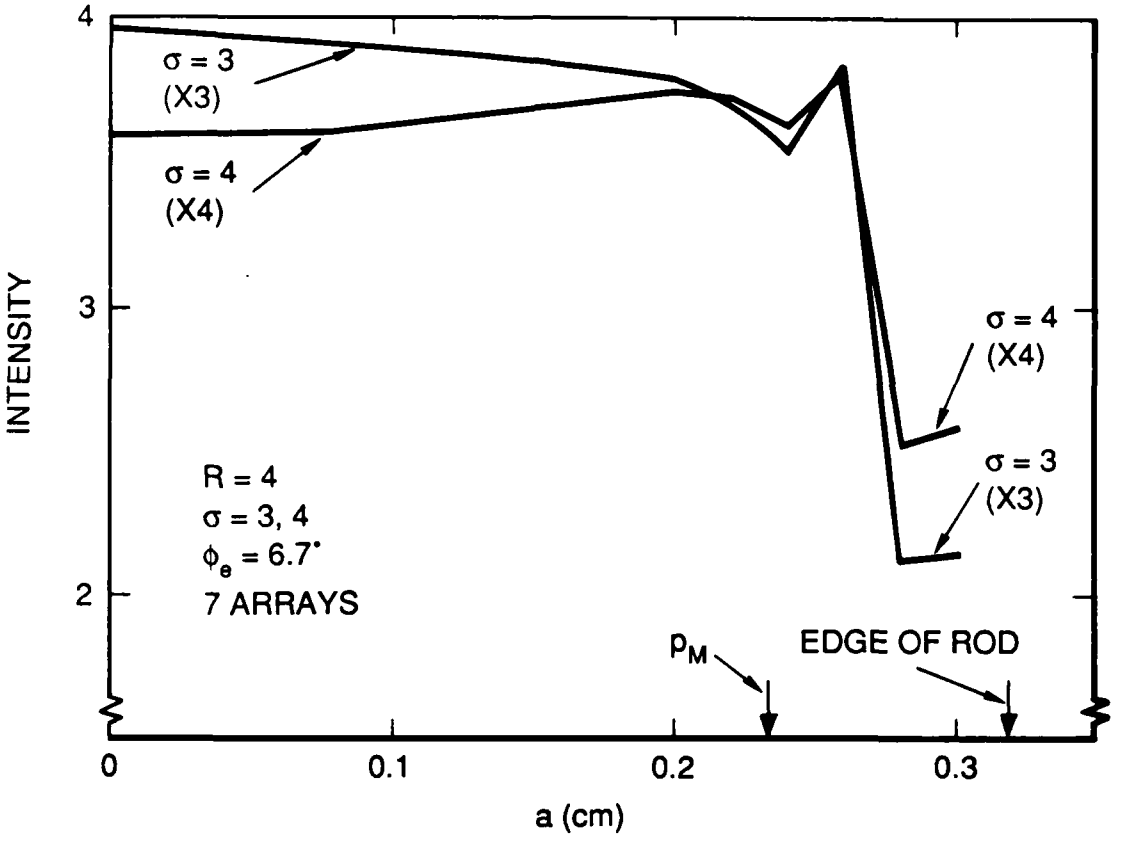

88-7504

Figure 10. Radial distributions for near optimum parameters aimed at uniform distribution. (Multipass calculation.) These distributions are computed for P-polarization, and are not normalized to unit power per unit length from the source.

fairly well, especially in view of the fact that the reflective losses at the glass and YAG surfaces were not folded into the angular distribution of the pump in the optimization analysis. (The curves in Figure 10 were calculated along the line $\alpha = 0$ i.e. along a radius aligned with one of the seven arrays. If the calculations had been performed at any different α, the differences would have been undetectable on the curves until a reached 0.24. The observational results would probably show more symmetry than the calculations.)

The rays that leave an array spread over a significant arc on arriving at the reflecting surface, as illustrated in Figure 9. The spread is shown in Figure 11 for a typical geometry. If ϕ_e is small, say 2 degrees, the energy transmitted through the rod would be concentrated over a range of about 25 degrees. The dependence of this range on geometry has not been investigated. If the range is small it makes sense to have an odd number of arrays if they are arranged inside the circle R (and imaged at R). Alternatively, the diode arrays might be outside the circle R and imaged onto slits in the reflector. The choice between mounting the diode inside the reflector (with lenses forming virtual images) and outside (with real images at the slits) would probably be made on the basis of mechanical convenience and simplicity (favoring outside mounting).

The conditions for uniform pumping in the region of the axis of the rod as expressed in Eq. 28 and Fig. 8 is modified somewhat in the multipass case, owing principally to the effective broadening of the antenna pattern in Eq. 30. Again a Gaussian antenna pattern exp $-(\phi/\phi_e)^2$ will be used to illustrate the case, and again the relevant expressions in ϕ and x will be expanded as far as second order in these variables with x equal to $(nR/n_1)\phi$. Expansion of the right side of Eq. 31 gives

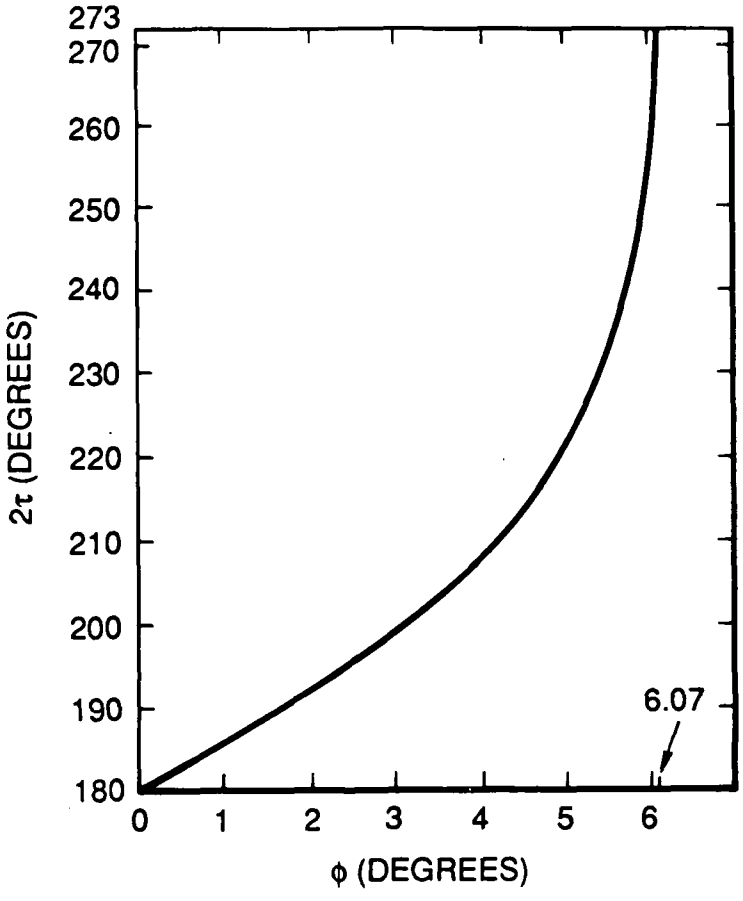

88-7507

Figure 11. Angular positions of rays after one pass. The geometry is that shown in Figure 5.

$$\rho = \rho_o + \rho_2 \phi^2 \qquad (32)$$

with $\rho_o = G T_o^2 \, e^{-2\sigma r_1}$

and $\rho_2 = G\{2T_o T_2 + T_o^2 (nR/n_1)^2 (\sigma/r_1)\} \, e^{-2\sigma r_1}$

In these expressions T_o *and* T_2 *come from the expansion:*

$$\prod_j T(\beta_j) = T_o + T_2 \phi^2 \qquad (33)$$

where $T_o = \prod_{j=1}^{M-1} t_j$,

and $T_2 = -2 \, n^2 R^2 T_o \prod_{j=1}^{M-1} (1 - t_j)/(t_j n_j n_{j+1} r_j^2)$

(See Eq. 15 for the definition of t_j*.)*

This expression for T_2 *is valid for S-polarization. It must be multiplied by the factor (-2) for P-polarization.*

The antenna pattern in Eq. 30 to second order in ϕ *is:*

$$\frac{dW'}{d\phi} = \frac{\frac{dW}{d\phi}}{1 - \rho_o} \left\{1 - \left(\frac{1}{\phi_e^2} - \frac{\rho_2}{1 - \rho_o}\right) \phi^2\right\} \qquad (34)$$

Considering four pump beams as in Eqs. 27 and 28, we find the expansion:

$$I(x)/I(o) = 1 + \frac{x^4}{4}\left[(\sigma - b)^2 + b^2 + \frac{\sigma}{r_1} - \frac{2n_1^2}{n^2R^2}\left(\frac{1}{\phi_e^2} - \frac{\rho_2}{1-\rho_o} - \frac{T_2}{T_o} - \tfrac{1}{2}\right)\right] \tag{35}$$

Thus the left side of Eq. 28, which gives the condition for most uniform pump intensity variation near the axis, is to be replaced by

$$\phi_e' = \left(\frac{1}{\phi_e^2} - \frac{\rho_2}{1-\rho_o} - \frac{T_2}{T_o} - \tfrac{1}{2}\right)^{-\frac{1}{2}} \tag{36}$$

Here the last term, $\frac{1}{2}$, comes from $\cos\phi$ in the denominator of Eq. 25, T_2/T_o comes from the (M-1) factors $T(\beta)$ in the numerator, and the term $\rho_2/(1-\rho_o)$ comes from the multipass effect in Eq. 34. The results summarized in Figure 8 for example can therefore be readily extended to the multipass case by reading the vertical axis as ϕ_e', and subsequently evaluating ϕ_e by substituting the values of ρ_o, ρ_2, T_o and T_2 into Eq. 36.

The optimum pumping intensity distribution in terms of minimizing thermal equilibration times, or amplifying a single (Gaussian) mode input signal, would correspond to the coefficient of x^2 in Eq. 35 being negative. The corresponding relation amongst the design parameters may be readily found and expressed as a set of curves like those of Fig. 8.

Application of the Theory.

One way to use the theory above is to consider a laser rod and water jacket of specific radii, such as those values shown in Figure 5; and then to regard R and ϕ_e *as adjustable parameters in an exercise aimed at producing a relatively uniform pumping intensity profile in the middle of the rod. This implies that whatever the antenna characteristic width is in the diode laser arrays chosen for pumping, one can modify it to the desired value by use of a lens, and place to at the desired radius by straightforward design. Figure 12 illustrates possible methods for this modification. Eq. 28 (with the left side replaced by* ϕ_e' *as defined in Eq. 36) may be regarded as a functional relation between R and the optimum value of* ϕ_e *for various values of* σ *. The quantity b captures the focussing effects of the media from the pump source to the rod. The equations have been programmed in BASIC on our IBM PC. OPTIM.SIN and OPTIM.TAN give the optimum* ϕ_e *for given values of R for S and P polarizations respectively. An example of the results is given in Table I for the geometry of Figure 5 (with variable R), using S-polarization. (Fig. 8 contains the same kind of data.) The reflectivity of gold is about 0.974 at 0.8 micron wavelength. The computations have assumed a wall reflectivity of 0.95, i.e. roughly twice the loss of a perfect gold coating on a polished surface. The effective reflectivity is reduced by the presence of the entry slits if external focussing optics are used, or by the internal optics. If internal optics are used in conjunction with reflecting walls, these optical components should obviously be very small.*

The angles tablulated as ϕ_e*(3 or 5) are the characteristic antenna widths of optimum uniformity (according to Eqs. 28 and 36) near the axis of the rod in cases where* σ *is 3 or 5 respectively. It is seen that higher absorption coefficient, which tends to lower the illumination on the axis compared to that at the surface, requires*

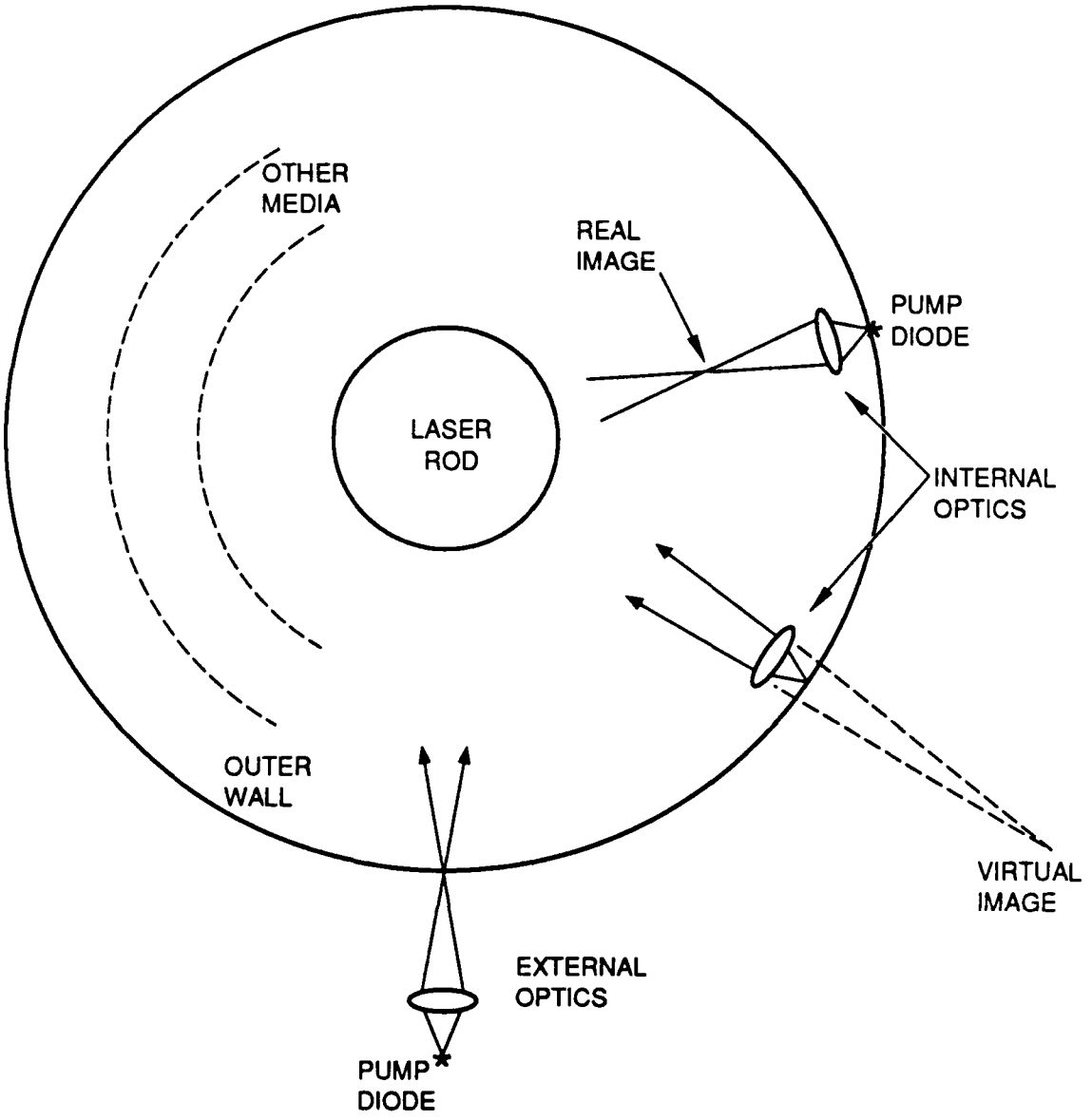

C88-8953

Figure 12. Adjustment of source position radius R and antenna width ϕ_e by use of internal or external optics.

TABLE I

OPTIMIZATION OF PARAMETERS

The Geometrical Parameter b, Optimum ϕ_e , and Error Function Argument for Various Values of R. The Fraction of Power Radiated in Angles less than the Critical Angle is given by Erf(x). The Absorption Coefficient is 3 cm^{-1} in x(3), $\phi_e(3)$ and 5 cm^{-1} in x(5), $\phi_e(5)$. The Reflectivity of the Wall is 0.95.

R	b	$\phi_e(3)$	x(3)	$\phi_e(5)$	x(5)
1	0.0349	31.97	.783	22.68	1.104
4	-1.332	6.74	.901	4.91	1.236
10	-1.606	2.57	.944	1.90	1.279
50	-1.752	0.500	.970	.372	1.304
500	-1.784	0.0497	.975	.0370	1.310
-50	-1.825	0.493	.982	.368	1.317
-10	-1.970	2.40	1.01	1.81	1.343

smaller antenna width ϕ_e as expected. The pumping efficiency, i.e. the fraction of diode laser power absorbed in the rod, contains a factor that accounts for the fraction of radiation at angles less than the critical angle, which is the error function of $\phi(critical)/\phi_e$. This ratio is denoted by x in the tables. Both the critical ϕ and ϕ_e decrease with increasing R(effective source radius) but x increases. From the tablulated values for R = 500 cm it is seen that a collinated beam is better than a diverging one; and from the values for R = -50 and -10, it is clear that a converging beam is better still in terms of this efficiency factor. However, the internal optics make assembly and adjustment more difficult.

The approach that we have used for deducing the conditions for most uniform pumping near the axis is based on a quadratic approximation for the intensity. Obviously the assumed Gaussian antenna pattern has a more rapid fall-off, and the result is that the parameters deduced from the theory tend to give a maximum on axis as shown in Fig. 6 and the upper curve in Fig. 10. If a very uniform pumping intensity is desired the approach to be used is that suggested by Fig. 10, which is to select a value of ϕ_e that belongs to a somewhat smaller σ (absorption coefficient). However this lowers the value of x. The value of Erf(1.16) is 0.90, so that x should be greater than 1.16 if this efficiency factor is to be at least 90 percent. (As in most laser applications, while mathematical calculations are simplified by the assumption of a Gaussian intensity profile, a more desirable profile is one that has a flatter top and steeper sides.)

Computer programs for determining the pump distribution are readily developed. The theory is simple enough for programs to be written on a hand-held calculator, such as the Hewlett Packard HP 41CV. The calculator is slow but it is has the advantage of "double precision" built in automatically, which increases the reliability of

the programs against crashes. Our IBM PC BASIC program "AUTOPUMP" generates the pump intensity distribution within the basic sector at eleven radii (including zero), and eleven angles at larger radii and six angles at the lower radii where the angular variation is smaller. The program can handle up to 10 concentric media (and more, as modified by Pharos). This program and its variants have been exercised extensively and many results that should be obvious a priori are revealed. Some of these observations are as follows.

The inner boundary of the caustics is at radius $a = n_2 r_1 / n_1$. *The area inside this radius contains* $(n_2/n_1)^2$ *of the cross section, and one can make the intensity of pump light quite uniform in this region. Some typical values of the cross section area ratios are given in Table II. The relative non-uniformity in the outer part of the rod has two principal causes, the caustic and the proximity of the sources. As an extreme example of the latter, if the sources are close to the rod and have narrow antenna patterns, and if in addition the absorption through the rod is large, then the pump intensity shows a set of strong peaks around the outer portion of the rod each facing a pump source. Obviously, increasing the number of sources on the circle improves the uniformity. At least three sources would seem to be necessary. Four or five would be better.*

Pumping Efficiency.

The light emitted by the diode lasers is absorbed in the laser rod, the reflecting walls of the laser head, and in the cooling fluid (e.g. water) and its jacket (e.g. glass of fused quartz). The absorption in pure water is about 0.023 cm^{-1} *at 0.800 micron wavelength, and will account for about one percent of the pump light absorption. Of the total pump light available a fraction* η *is absorbed in the laser*

TABLE II

Area with Smooth Pump Intensity - Inside the Caustics

Medium I (n_1)	*Medium II* (n_2)	*Area Ratio* $(n_2/n_1)^2$
YAG (1.823)	*Water* (1.333)	*0.53*
YAG	*Ethylene Glycol* (1.427)	*0.61*
YAG	*Quartz* (1.453)	*0.66*
YAG	*50-50 Eth. Gly.-Water* (1.380)	*0.57*
YLF (1.634_o, 1.631_e)	*Water*	*0.67*
YLF	*50-50 Eth. Gly.-Water*	*0.71*

rod. The quantity η is called the pumping efficiency here, and it can be calculated with accuracy consistent with that of the pumping intensity calculations, i.e. limited by the assumptions that go into Eqs. 30 and 31 in the multipass analysis. There are two simple approaches to the calculation of η . One is to figure out the absorptions of a single ray as it makes successive passages through the rod. The other is to integrate σI over the volume of the rod.

The successive absorptions in the rod and in the surface of the reflector at radius R respectively can be added using the multipass analysis. The notation used in Eq. 31 is simplified by expressing the exponential factor as $e^{-\sigma S(\phi)}$ *and by*

$$T(\phi) = T(\beta_1)\ T(\beta_2)\ T(\beta_3)\ \ldots$$

The absorbed powers are:

$$P(rod) = \int_{-\Phi}^{\Phi} (1-\rho)^{-1}\ T(1-e^{-\sigma S})(dW/d\phi)d\phi \qquad (37)$$

$$P(surface) = \int_{-\Phi}^{\Phi} (1-\rho)^{-1} T^2 (1-G)\ e^{-\sigma S}(dW/d\phi)d\phi \qquad (38)$$

These formulae count only the light radiated at angles less than Φ , the antenna pattern cut-off or ϕ_M *, whichever is smaller. If* ϕ_M *is smaller, the pumping efficiency contains the factor* $W(\phi_M)/W(\Phi)$ *(assuming that W is symmetric) which accounts for pump light that cannot reach the laser rod. Pump light reflected or scattered at the interfaces between successive media has been neglected in Eqs. 37 and 38, thus representing a deficit of*

$$P(neglected) = \int_{-\Phi}^{\Phi} (1-\rho)^{-1}(1-T)(1+Te^{-\sigma S})(dW/d\phi)d\phi \qquad (39)$$

Some of this will find its way into the rod.

From Eq. 34 it is clear that the pump light intensity at the center of the rod is increased by the factor $(1 - \rho_o)^{-1}$ by providing a reflecting surface at radius R. The total increase in pumping due to the reflecting surface is found by computing Eq. 37 with the appropriate functional form for $p(\phi)$ and dividing by the same integral evaluated with ρ equal to zero: The result is somewhat greater than $(1 - \rho_o)^{-1}$ because the function $dW'/d\phi$ is broader than $dW/d\phi$ as seen in Eq. 34; but the factor $(1 - \rho_o)^{-1}$ is a good approximation. (Recall that ρ_o is the total attenuation along the central ray.)

Consider the following example:

$n_1 = 1.823$, $r_1 = 0.3175$ cm, $\sigma = 3\ cm^{-1}$ (YAG)

$n_2 = 1.333$, $r_2 = 0.5$ (Water)

$n_3 = 1.5$, $r_3 = 0.65$ (Glass water-jacket)

$n = 1$, $R = 4$ cm (Location of diodes)

$dW/d\phi = \exp -(\phi/6.7\ deg.)^2$

$\phi_M = 6.073$ deg.

$G = 0.974$ (reflectivity of gold)

Pump Polarization: P

$T(o) = .9336$ (Air-glass-water-YAG)

Then $\rho_o = 0.1263$, and $(1 - \rho_o)^{-1} = 1.1446$.

Of the diode power radiated into angles less than 6.073 deg. the fraction 0.9365 is absorbed in the YAG rod. If G = 0 (single-pass pumping) the fraction absorbed is 0.7773. The pumping is increased by the factor 0.9365/0.7773 which is 1.2048, which is to be compared to the simple approximation that gives 1.1446. Notice that $\exp(-2\sigma r_1)$ is 0.1488 while the corresponding quantity for the critical ray is 0.2727. The pumping efficiency 0.9365 is now multiplied by $W(\phi_M)/W(\Phi)$ which is the error function erf(6.073/6.7) = 0.800. Multiplying this by 0.9365 drops the efficiency to 0.75. On the other hand, much of the drop from unity to 0.9365 is due to having T(o) = 0.9336. (T increases with increasing ϕ because of the polarization chosen.) Without Fresnel losses the fraction absorbed would go from 0.9365 to 0.9945. Thus the Fresnel reflection losses account for 5.8 percent.

In summary, the various pumping efficiency factors in the chosen example are as follows.

Radiated into $\phi < \phi_M$ (Gaussian):	0.800
Fresnel for P-polarization:	0.9417
Absorption in rod (multi-pass):	0.9945
Net efficiency:	0.75
Multi-pass/Single pass	1.20

The net efficiency should be multiplied by the approximate additional factors 0.99 to account for absorption in the cooling water, and 0.95 if the polarization is S instead of P. These will bring the net efficiency

down to 0.70. The biggest loss factor is that due to the lost power in the Gaussian wings of the antenna pattern of the diodes, and many other numerical examples have verified this same effect.

The factor G that occurs in Eq. 38 and in Eq. 31 for ρ (which occurs in Eqs. 37 and 38) refers to the reflectivity of the wall, but also accounts for the obscuration of the reflecting wall by any internal optics. As an example, if we choose R = 500 cm this implies that we have internal optics in front of the diodes as shown in Fig. 12. A reasonable value to use for G in this case would be 0.9. Since the reflectivity of clean gold is 0.974 at 0.8 micron, a value of G higher than 0.9 can be assumed for R = 4 cm, especially if the diode lasers are outside the gold reflector, with the pump light entering through slits. This case also is shown in Fig. 12. Because the effective value of G is larger, R = 4 cm gives a higher η than R = 500 cm. The intensity plots of the R = 50 cm case are shown in Figure 13.

We have assumed in these computations that the light reflected from the interfaces is lost, whereas it is reflected back from the walls towards the rod again. Eq. 31 is readily modified to account for this additional feedback. The result is:

$$\rho(\phi) = (1 - t + te^{-\sigma S})G \qquad (40)$$

where

$$t = \prod_j T(\beta_j)$$

and $$S = 2\left[r_1^2 - \frac{n^2 R^2}{n_1^2} \sin^2 \phi\right]^{\frac{1}{2}}$$

In order of importance, we can list the measures recommended for high pumping efficiency.

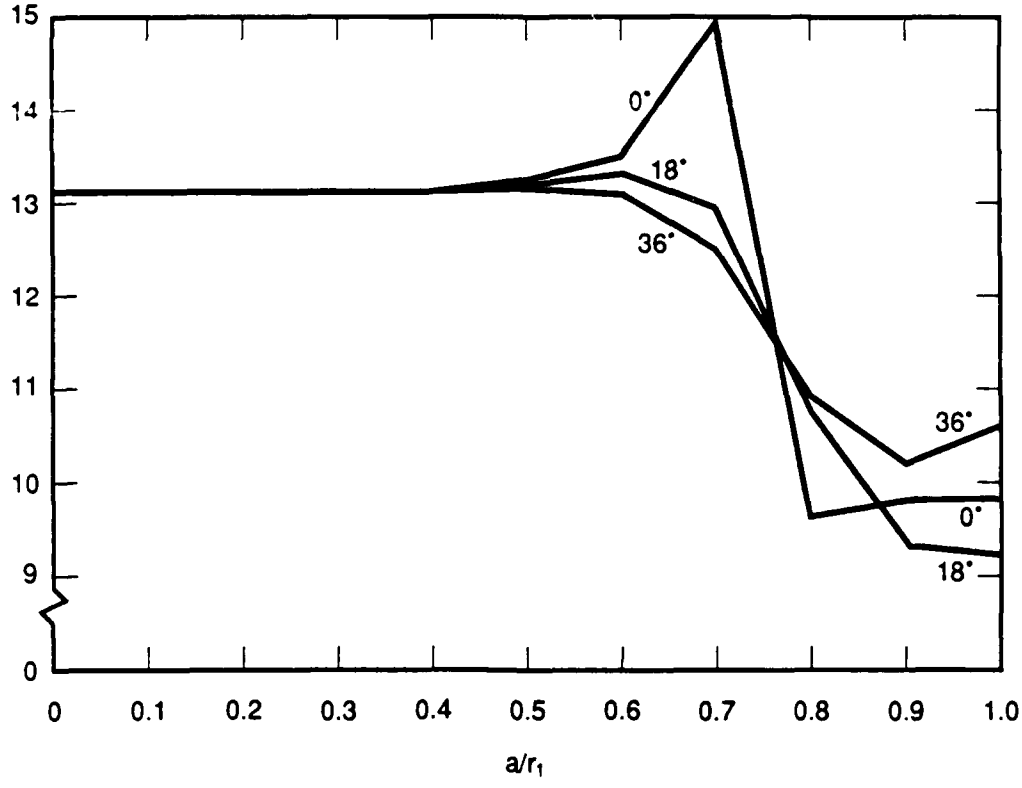

C88-8954

Figure 13. Pump intensity distributions for R = 50 cm at different angular positions, corresponding to the "Virtual Image" case in Fig. 12. Equally uniform distributions can be generated by computation of the other two cases with optimization of ϕ.

(i) Use a highly reflecting wall for pumplight feedback.

(ii) Use optics external to the reflecting wall for controlling the pump beam characteristics, and have the pump light enter through narrow slits in the wall.

(iii) Design the optics so as to bring light from the wings of the antenna pattern into the central portion, so that it can enter the rod.

(iv) Apply anti-reflection processing to water-jacket, lenses, and other surfaces intersecting the pump rays.

(v) Minimize the number of concentric media in the design so as to reduce losses from the pump to the laser rod.

(vi) As an experimental matter, check the absorption coefficient of the pump light in the cooling liquid.

The second method of calculating the efficiency is outlined below. The intensity I is given directly in units of watts/cm^2 in our computer program, where the assumed source strength is 1 watt/cm. When I is multiplied by σ , the absorption coefficient, the result σI is the power absorbed per unit volume (watts/cm^3). Since $I(a,\alpha)$ is computed at large number of points it is a simple matter is perform the surface integral of I over the cross section of the rod, which yields in watts/cm the power absorbed in the rod. This can be divided by the power radiated, N watts/cm from all pump sources, to give the pumping efficiency. The formula is

$$\eta = N^{-1} \int \int I(a,\alpha)\, a\, da\, d\alpha$$

$$= 2 \int_0^{\pi/N} I(a,\alpha)\, a\, da\, d\alpha \qquad (41)$$

This method of calculating η is not as simple as the first method, but is a simple addition to the computer program that calculates intensity distributions. For comparison we calculated the η for the last case discussed above and got 0.7335 using Eq. 44 and 0.7492 using Eq. 37. (So far we have not found the cause of this discrepancy.)

Axial Propagation.

The angle δ that the ray makes with the transverse plane has so far been assumed to be zero. Relaxing this restriction makes Figure 2 a projection in the (r,θ) plane of the ray in three dimensional (r,θ,z) space. Thus the angles β_j and β'_j are defined in relation to the projections of the rays on to the transverse plane. With the cylindrical symmetry assumed in this treatment, a ray crossing a boundary between media n_1 and n_2 will make angles $(90^0 - \delta_1)$ and $(90^0 - \delta_2)$ with the cylinder generator; and phase matching along this generator leads immediately to

$$n_1 \sin \delta_1 = n_2 \sin \delta_2 \qquad (42a)$$

While the fact that the two rays and the normal are coplanar gives

$$\sin \beta_1 / \sin \beta_2 = \tan \delta_1 / \tan \delta_2 \qquad (42b)$$

The ray tracing thus gives:

δ_1 *= constant up to the boundary, and*

$r \sin \beta_1$ *= constant up to the boundary, so that* β_1 *is function of r.*

Then Eq. 42a gives a new δ(called δ_2) and Eq. 42b gives a new β(called β_2) . Thence δ_2 and r sinβ_2 remain constant up to the next boundary. The net result is that the formula for each β_j and β'_j in Eq. 1 (as used in Eq. 5a and 5b for example) has (n/n_j) replaced by $(\tan \delta_j/\tan \delta)$, which is equivalent to the substitution:

$$\frac{n}{n_j} \rightarrow \left(\frac{n}{n_j}\right) \cos \delta / \left[1 - \left(\frac{n}{n_j}\right)^2 \sin^2 \delta\right]^{\frac{1}{2}} = M_j(\delta) \; ; \qquad (43)$$

where δ is defined at the diode array source along with ϕ as the angular coordinate in the antenna pattern. (Recall that n is the index of refraction of the outermost medium.)

In propagating from a diode array to the field point (a,α,z) inside a laser rod, the ray advances axially through the distance

$$\Delta z = z - z_i = \sum_{j=M}^{1} (r_j \cos \beta_j - r_{j-1} \cos \beta'_{j-1}) \tan \delta_j \qquad (44)$$

where the last r_{j-1} and β'_{j-1} are a and $\sin^{-1}(p/a)$ respectively, and where the last term will also have a "plus" sign rather than "minus" in the case of $\alpha = \alpha_2$ (the second intersection of the ray with the cylinder r = a). Here z_i and z are axial coordinates at the source and the field point respectively. The β_j are all found from Eq. 1 with substitution of Eq. 43, while the δ_j in Eq. 44 are given by Eq. 42a as

$$\sin \delta_j = (n/n_j) \sin \delta \; , \qquad (42c)$$

or

$$\tan \delta_j = M_j \tan \delta \qquad (42d)$$

It is necessary in the three dimensional problem to find both δ *and* ϕ *that identify the ray through the field point. The equations to be solved for* (ϕ,δ) *are first Eqs. 5:*

$$\alpha_1 = \phi_i + \phi + (\beta_j - \beta'_j) - \gamma \qquad (5a)$$

and

$$\alpha_2 = \alpha_1 - \pi + 2\gamma \qquad (5b)$$

where

$$\sin \beta_j = (nR \sin \phi/n_j r_j)\, M_j$$

$$\sin \beta'_j = (nR \sin \phi/n_{j+1}\, r_j)\, M_j$$

$$\sin \gamma = (nR \sin \phi/n_1 a)\, M_j = p/a \ ;$$

and then Eq. 44:

$$z = z_i + \sum_j (\ldots) M_j \tan \delta \ . \qquad (44)$$

Various computational methods are available for solving for (ϕ,δ) *such as Newton's method, generation of look-up tables, and successive approximations such as* $(\phi^o,0)$, (ϕ^o,δ^o); (ϕ^1,δ^o). (ϕ^1,δ^1), *etc. where* (ϕ^{n+1},δ^n) *solves Eq. 5 with* δ *fixed at* δ^n *and* (ϕ^n,δ^n) *solves Eq. 44 with* ϕ *fixed at* ϕ^n .

Taking account of the axial component of propagation will have little effect on the estimates of pump intensity obtained by the two-dimensional propagation. In the multipass situation involving reflection of the transmitted light back into the rod, there will be a walkoff effect that will mainly smooth out the intensity variations between

neighboring arrays; but the various ray angles (and associated intensity calculations) will be well approximated by the two-dimensional theory. The easiest way to see all this is to combine Eqs. 42a and 42b to give:

$$\frac{\sin \beta_1}{\sin \beta_2} = \left[\left(\frac{n_2}{n_1}\right)^2 + \left\{\left(\frac{n_2}{n_1}\right)^2 - 1\right\} \tan^2 \delta_1\right]^{\frac{1}{2}} \qquad (45a)$$

which for small δ_1 *can be approximated by*

$$\frac{\sin \beta_1}{\sin \beta_2} = \frac{n_2}{n_1} + \frac{1}{2}\left(\frac{n_2}{n_1} - \frac{n_1}{n_2}\right) \tan^2 \delta_1 \qquad (45b)$$

This will be less than a one percent deviation from n_2/n_1 *for the range of* δ *(a few degrees) that will occur.*

Recall that the two-dimensional intensity formula (Eq. 10) has on its right side terms of the type dW/dw multiplied by the transmission coefficient T. The numerator may be considered to be $(dW/d\phi)d\phi$ *, representing the power radiated by the source i into the angle* $d\phi$ *; while the denominator similarly is* $(a^2 - p^2)^{\frac{1}{2}} \left|d\alpha/d\phi\right| d\phi$ *, representing the line element perpendicular to the ray through which the power dW flows. In three dimensions the formula is readily patched by changing the numerator to* $(\partial^2 W/\partial\phi\partial\delta)d\phi d\delta$ *and putting the additional factor* $(\partial z/\partial\delta) \cos \delta_1 d\delta$ *in the demoninator in order to generate the area element through which power dW flows. The net result is:*

$$I(a,\alpha,z) = \sum_i \frac{T_i (dW_1/d\phi)(dW_2/d\delta)}{\{a^2 - (M_1 R \sin \phi)^2\}^{\frac{1}{2}} \left|\frac{\partial\alpha}{\partial\phi}\right| \{1 - (n \sin \delta/n_1)^2\}^{\frac{1}{2}} \left(\frac{\partial z}{\partial\delta}\right)} \qquad (46a)$$

Here we have replaced the second derivative of W in the numerator by the product of the two first derivatives on the assumption that $W(\phi,\delta)$ factorizes, which is almost certainly the case with diode arrays. Since there is not much depolarization for small δ the exact (ϕ,δ) - dependence of T_i are not shown. The values given by Eq. 11 and 12 are close enough.

Eq. 46a is good for a source having zero extent in the z-direction, and needs to be modified for a diode array. The z-coordinate in the array is written z_i as in Eq. 44. If the array is coherent the radiation at the field point will be of near-field character, and the factor $dW_2/d\delta$ in the numerator combines with $(\partial/\partial\delta)(z-z_i)$ in the denominator to give $dW_2(\delta)/dz_i$, which characterizes the source radiation at direction δ . (In Equation 46a, z_i was assumed to be zero.) A given field point may be illuminated by two separate coherent arrays if the arrays each radiate at two distinct angles (e.g. $\pm\ \delta_i$) .

If on the other hand the array is incoherent one must add the illuminations from different elements along the array, and form a sum over z_i of terms of the type that contain δ in Eq. 46a. Expressing the result as an integral gives the factor

$$\frac{\{\partial W_2/\partial z_i + (\partial W_2/\partial\delta)\,|\partial\delta/\partial z_i|\}}{\{1 - (n \sin\delta/n_1)^2\}^{\frac{1}{2}}}\, dz_i \qquad (46b)$$

where δ is given as a function of z_i for fixed ϕ. The factors containing ϕ in Eq. 46a remain the same.

Convergent Pump Beams and Finite Apertures.

The analysis referred to in Fig. 1 needs to be extended to cover the case where the light from each diode array is made weakly convergent by passing through a positive lens. The resulting beam passes through an aperture in the reflecting surface at radius R. (Fig. 1 is still appropriate for a diverging beam; but if the reflecting surface is located at a radius less than that locating the virtual sources, the reflector will have holes in it, and the present analysis can be used to treat this case as well.) Fig. 14 shows the aperture A_1AA_2 *in the reflector, with pump light converging towards a point C on the diameter at the distance D from the entry point A. Angular positions on the wavefront are labeled by* χ *referred to C (towards which the rays are directed), while the aperture itself is labeled by the variable* ϕ_i*, with* ϕ_i *equal to* ϕ_{io} *at the center. The index i counts the pump sources.* ϕ_i *is the same quantity as* θ_M *in Eq. 5a. As before* $\phi(i)$ *abbreviated to* ϕ*, denotes the angle between the ray and the radius, and in accordance with the sign convention chosen, is positive as shown in the figure. There is a one-to-one correspondence between* ϕ *and* $(\phi_i - \phi_{io})$*, and between* ϕ *and* χ*. The offset of the ray projection from the center 0 is*

$$R \sin \phi = (D - R) \sin \chi \tag{47}$$

while

$$\phi_i - \phi_{io} = \chi + \phi \tag{48}$$

$$= \phi + \sin^{-1}\left\{\frac{R \sin \phi}{D - R}\right\} \tag{49}$$

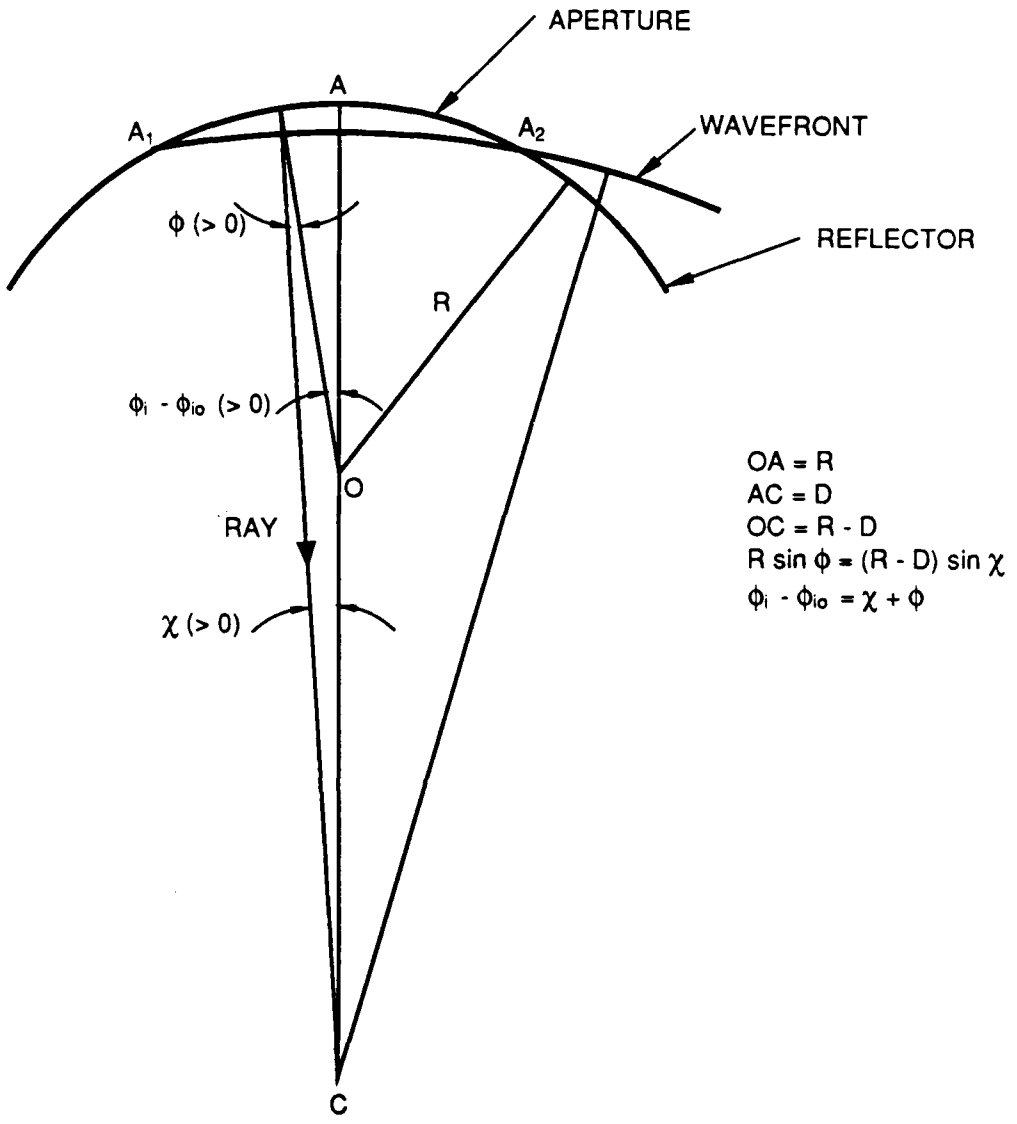

C88-8955

Figure 14. Geometry of wavefront converging on C passing through aperture A_1AA_2 in reflector centered on O. ϕ_i labels the point in the aperture at which the ray direction is ϕ (shown positive). χ labels the point on the wavefront in terms of which the antenna pattern of the source is defined.

These relations hold irrespective of the sign of D or its size in relation to R. The interesting case for D positive is with D large compared to R so that no focus forms in the rod. Thus from Eq. 49, $d\phi_i/d\phi$ is positive.

Notice also that the pump source distribution expressed in terms of χ is readily transformed to the variable ϕ :

$$dW = (dW/d\chi)\, d\chi = (dW/d\chi)(d\chi/d\phi)d\phi = (dW/d\phi)d\phi$$

so that Eq. 10 for the intensity at a point in the rod is still valid. For the small values of ϕ and χ involved, Eqs. 47 and 49 are essentially linear relations amongst the variables.

The method for finding the value of ϕ corresponding to α for a given radius a is now a little different. Previously, given α , we imagine a horizontal line at height α on Figure 4 intersecting the curve $\alpha(\phi)$ to identify ϕ . The algebraic problem to solve was Eq. 7:

$$\alpha(\phi) - \alpha = 0$$

The curves $\alpha(\phi)$ in Fig. 4 are drawn for $\phi_i = 0$, and have $+\phi$ as the horizontal axis. They are identical to plots of $(\phi_i - \alpha)$ versus $-\phi$. Now the problem is to find ϕ that solves Eqs. 7 and 49 simultaneously, i.e.

$$\phi_i - \alpha = \phi_i - \alpha(\phi) \qquad (7a)$$

and

$$\phi_i - \phi_{io} = \phi + \sin^{-1}\left\{\frac{R \sin\phi}{D - R}\right\} \qquad (44)$$

The method of solution is illustrated graphically in Fig. 15, from which it is clear that the problem to be solved is to find ϕ that satisfies the following equation:

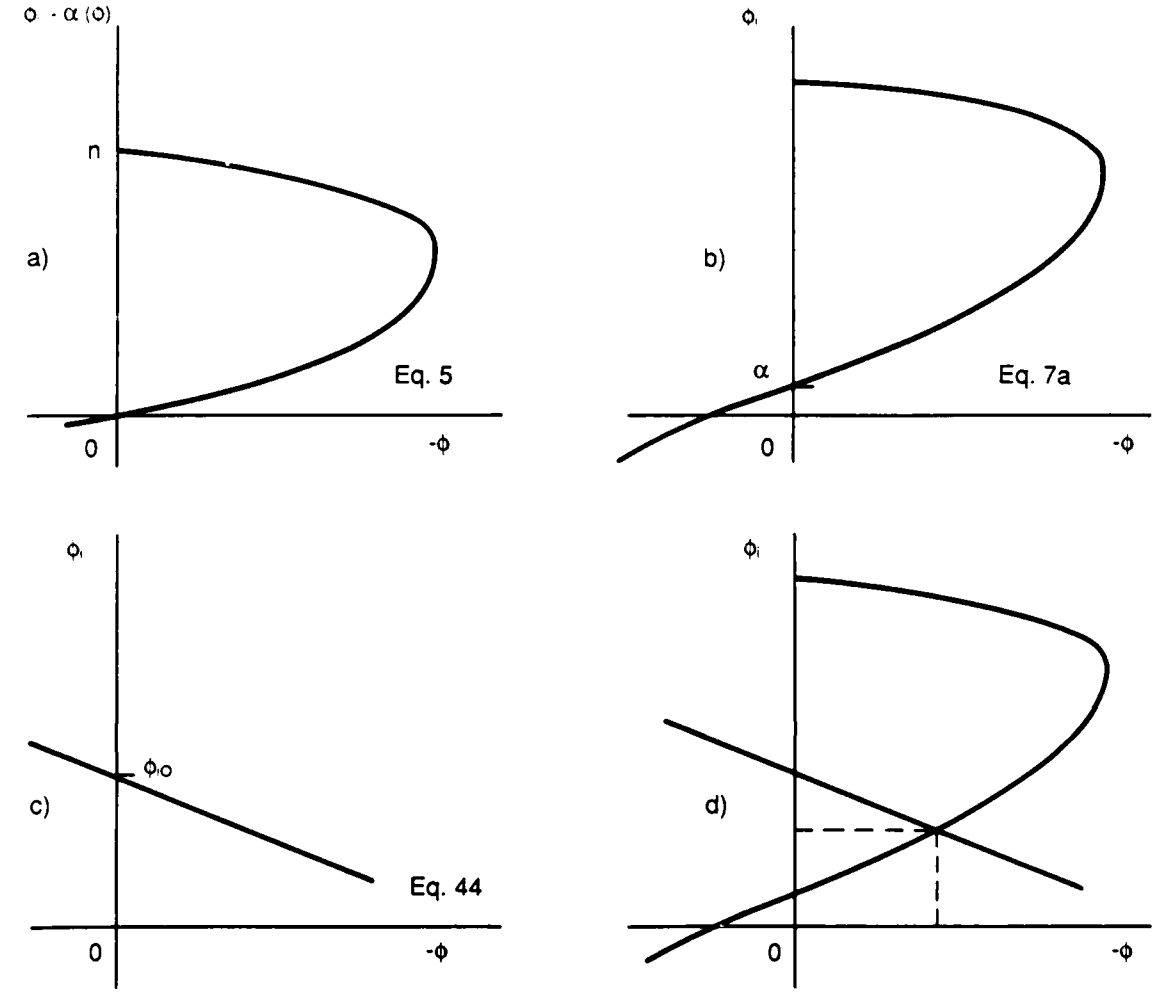

88-8956

Figure 15. Graphical illustration of the simultaneous solution of Equations 7a and 49. a, b, c illustrate Eqs. 5, 7a, and 44 respectively. The solution (ϕ, ϕ_i) is given by the intersection in d.

$$0 = [\phi_i - \alpha(\phi)] + \alpha - [\phi_{io} + \phi + \sin^{-1}\{\frac{R \sin\phi}{D - R}\}] \qquad (50)$$

The quantity in the first square brackets is the function obtained from Eq. 5 by moving ϕ_i *(which is* θ_M*) to the left side of the equation and then reversing the sign. The next term* α *is a number giving the angular coordinate of the field point. The quantity in the second square brackets is the function* $\phi_i(\phi)$ *identified by Eq. 49. In shorter notation, Eq. 50 is*

$$0 = \sum_j \beta'_j(\phi) - \sum_j \beta_j(\phi) + \gamma(\phi) + \alpha - \phi_i(\phi) \qquad (50a)$$

Here the β'_j *and* β_j *are identified in Eqs. 1 and 5, and* $-\gamma$ *is the second to last term of Eq. 5a.*

After solving Eq. 50 for ϕ *it is an easy matter to apply Eq. 10 for the intensity. The terms in the numerator are now:* $T(dW/d\chi)$ $(d\chi/d\phi)$ *(where the subscripts i are dropped for simplicity). The denominator is now formally the same, but in the computation it is necessary to add to the formerly used expression for* $d\alpha/d\phi$ *the new term:*

$$d\phi_i/d\phi = 1 + d\chi/d\phi \qquad (51)$$

where we have used Eq. 48. A simple check on the theory is to treat the case shown in Figure 16, even though the pump waves are diverging in this case, because we already have the results in terms of the earlier analysis wherein C is located on the circle of radius R' *. Let* $-f(\phi)$ *represent the functional form in the first square brackets in Eq. 44; i.e. f is the expression given by Eq. 5. Then the modified form of Eq. 10 contains*

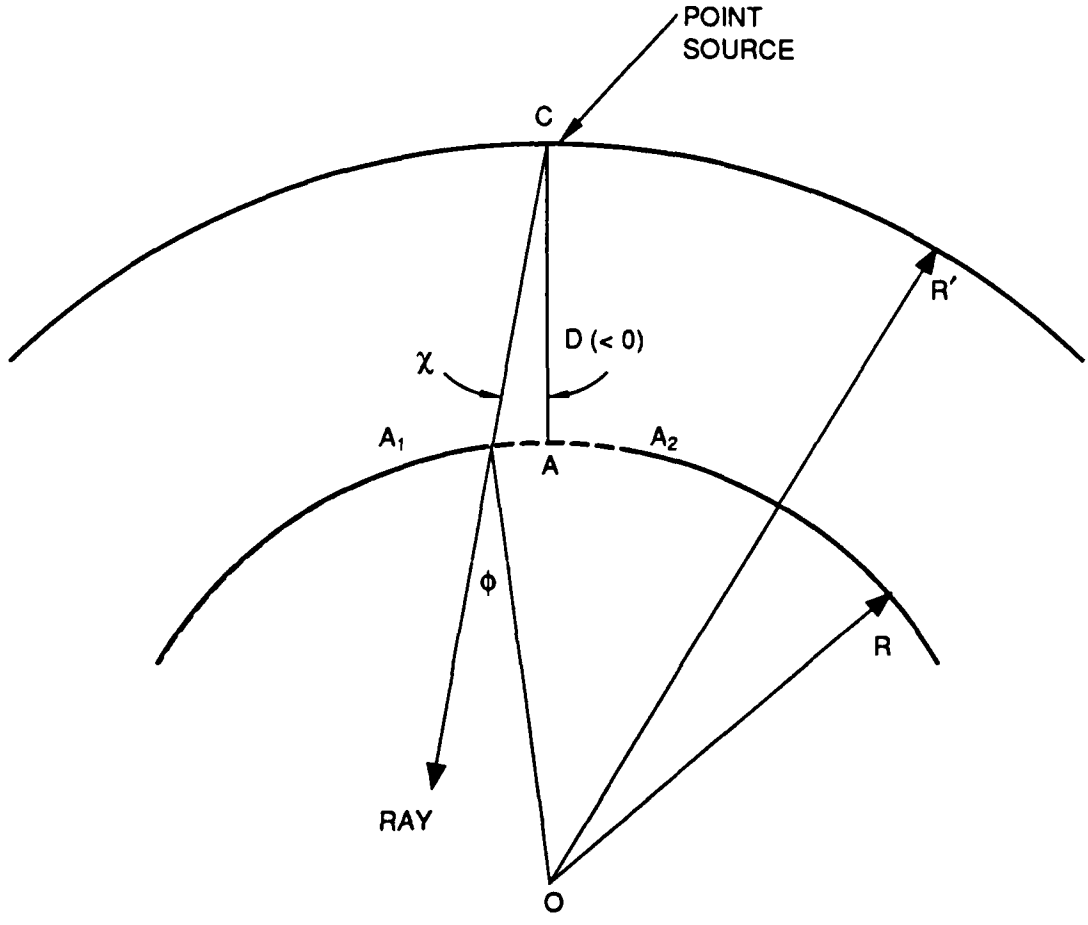

C88-8957

Figure 16. Geometry of aperture with diverging wave, where D is negative. The radius of the reflector is less than the radius of the surface containing the sources. Here R' replaces R in Eq. 1 and other equations in that section.

$$\frac{(dW/d\chi)(d\chi/d\phi)}{(d/d\phi)(f + \phi_i)} = \frac{dW/d\chi}{(d\phi/d\chi)(d/d\phi)(f + \phi_i)}$$

$$= \frac{dW/d\chi}{d\alpha/d\chi}$$

thus yielding the correct result referred to angles χ *at the source, as expected. The significance of this result is trivial and obvious when D is a small positive quantity (smaller than* $R - r_3$ *in the case of four concentric media), or any arbitrary negative quantity, because it means that we simply deal with the positions and antenna patterns of the pump diode images in all analysis. The real significance is that for large D (convergent beam from the source-lens combinations) the original formulae are all still good although R is assigned a negative value in all computations i.e. R is replaced by (R - D), which is now negative, and this new parameter is renamed R; and* χ *is renamed* ϕ *. Thus in most computations, where lens aberrations are unimportant, it will be unnecessary to deal with Eqs. 49-51.*

SECTION 2

CAUSTICS

The results of Section 1 can be applied readily to calculate the pumping intensity disribution inside a cylindrical rod very quickly, and probably quite accurately except in the neighborhood of the caustics. This section presents the elementary geometrical theory for predicting the location of the caustics, develops the wave theory for calculating the intensities in the regions where the geometrical theory fails, and discusses measures that reduce the anomalous intensities associated with the caustics.

Location of Caustics

A caustic is the locus of the point of intersection of neighboring rays, which are tangential to the caustic curve. In our notation the caustic is characterized by $d\alpha_2/d\phi$ *being equal to zero at fixed radius a. The existence of the caustics is confirmed immediately by plotting* $\alpha_2(\phi)$ *at the outer surface of the rod i.e. at* $a = r_1$*, as illustrated in Figure 17. The minimum of the curve shown locates the point where the caustic meets the surface. Minima on similar curves for successively smaller values of a determine polar coordinates along the caustic. Figure 18 shows the resutant caustic curves. The values of the coordinates for the upper curve are tabulated together with corresponding values of* ϕ *in Table III. The caustics can occur only for points* (a,α) *where a exceeds* p_M*, because there the* $\alpha(\phi)$ *curve has two branches as in Figure 4. The single branch curves of Figure 4 have no maximum or minimum value of* α *other than 0 and 180 degrees.*

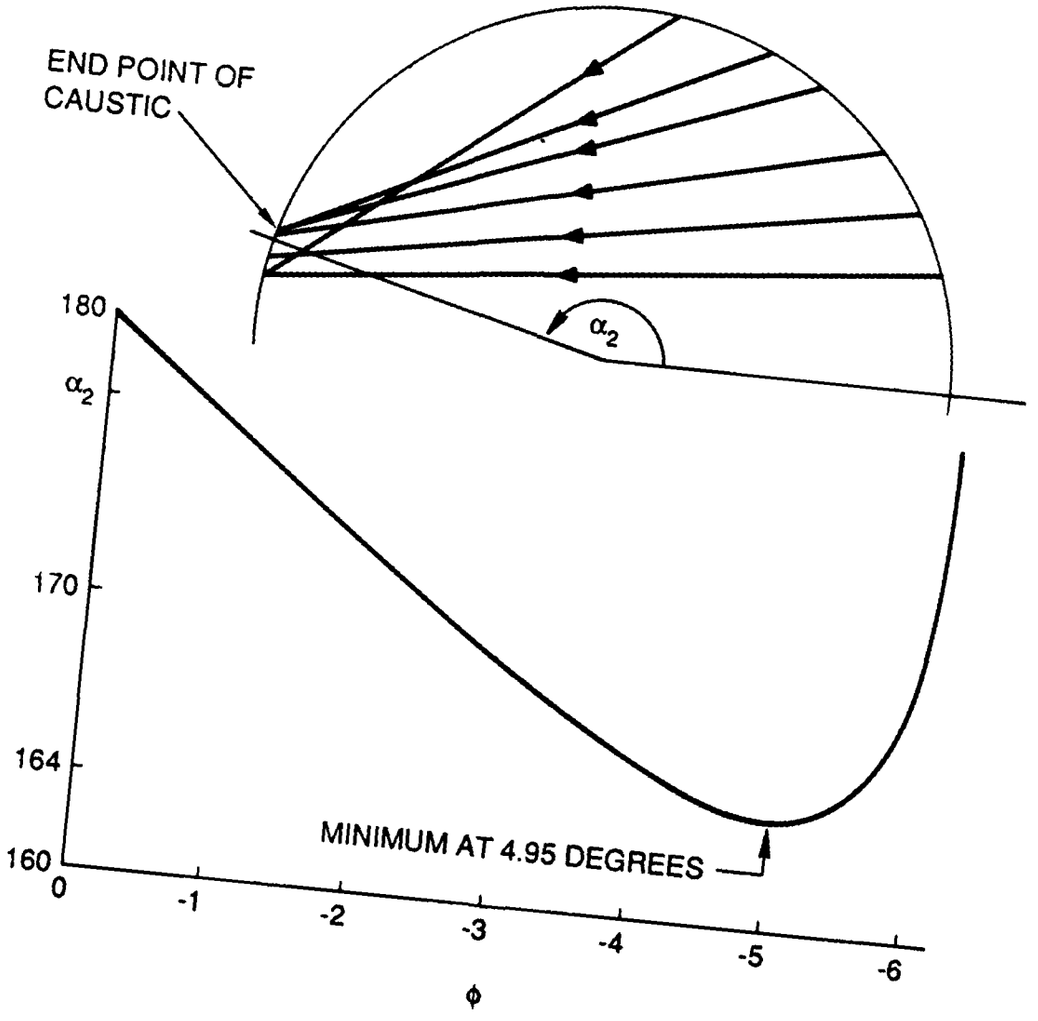

Figure 17. The minimum in the $\alpha_2(\phi)$ curve for $a = r_1$ locates the point at which the caustic touches the rod surface.

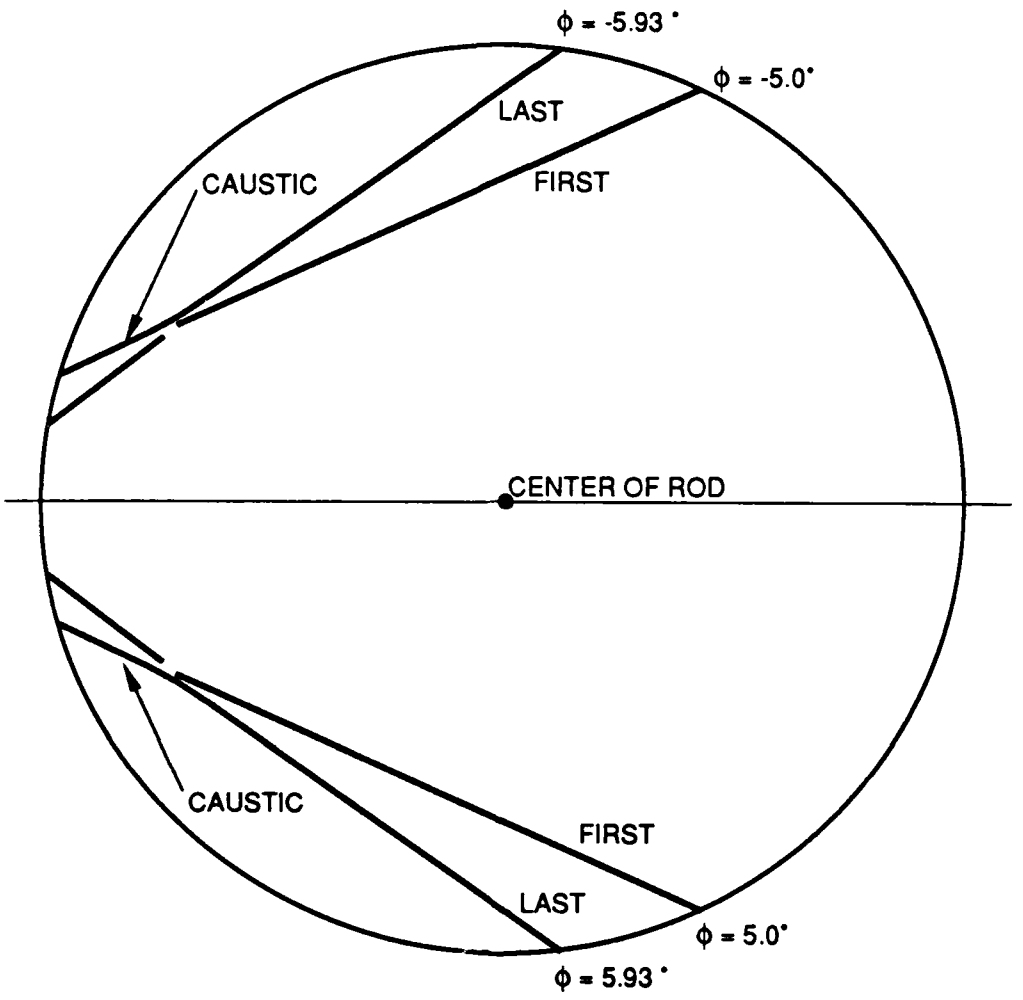

C88-8958

Figure 18. Caustic curves from a source at nR = 4, with geometrical parameters as defined in the previous subsection on pumping efficiency. The first and last rays on the caustics are also drawn.

TABLE III

Coordinates along the upper caustic of Figure 18

a (cm)	α (deg.)	ϕ (deg.)
0.3175	164.03	5.0
0.30	161.43	5.1
0.29	159.69	5.2
0.28	157.69	5.3
0.27	155.36	5.4
0.26	152.59	5.525
0.25	149.13	5.645
0.24	144.40	5.805
0.235	140.85	5.93

Caustics are to be expected in cases of practical interest in this work, and will not be eliminated by the addition of other concentric media to the simple geometry depicted in Figure 1. Referring to Eq. 8b for $d\alpha_2/d\phi$ it is seen that as ϕ approaches ϕ_M (which is $\sin^{-1}(n_2 r_1/nR)$) the second positive term within the braces approaches infinity as illustrated in Figs. 4 and 17, for which $a \geq p_M$. Therefore, unless $d\alpha_2/d\phi$ is positive at ϕ equal to zero, it will be zero somewhere in the interval $0 < \phi < \phi_M$. Substituting $\phi = 0$ in Eq. 8 with a equal to r_1 shows that the condition for no caustic is that

$$\frac{2}{n_1 r_1} < \frac{1}{n}\left(\frac{1}{r_3} - \frac{1}{R}\right) + \frac{1}{n_3}\left(\frac{1}{r_2} - \frac{1}{r_3}\right) + \frac{1}{n_2}\left(\frac{1}{r_1} - \frac{1}{r_2}\right)$$

for four media, with obvious extension to larger numbers of media. Replacing vacuum in any region $r' < r < r_2'$ by medium with index n' adds the negative quantity $\left(\frac{1}{n'} - 1\right)\left(\frac{1}{r_1'} - \frac{1}{r_2'}\right)$ to the right hand side of the inequality; and therefore the maximim value that the right hand side can have is $\left(\frac{1}{r_1} - \frac{1}{R}\right)$, with limiting value $1/r_1$. Comparison with the left side shows that we would need to have $n_1 > 2$, which occurs for the niobates amongst the common laser hosts, and maybe something else. For YAG or YLF or anything else with $n_1 < 2$, caustics will occur with the concentric geometry. The only ways to keep the caustics from forming in the gain region are to limit the range of angles from the pump source by suitable design of the coupling optics, or to have the laser rod material at radii exceeding $(n_2 r_1/n_1)$ undoped.

Because the upper branch of the α versus ϕ curve has the infinite slope at its extremity the inner end of the caustic is identified with the point at the angular break on curve 4 of Fig. 4, which is at the mid-point of the chord marking the critical ray (i.e. $\phi = \phi_M$). Each pump source generates two caustics symmetrically about its central ray. Caustics from different pump sources intersect, doubling locally the intensity anomaly. (With five pump sources the

angular positions of the intersections are zero and multiples of 72 deg.) We have no mathematical formula that generates the caustic curves, but it is a simple matter to construct a table of coordinates like Table III once a calculator has been programmed to generate $\alpha_2(\phi;a)$. The table then serves as a guide for selecting a cut through the geometrical optics caustic along which intensity can be computed.

In terms of the multipass analysis used in Section 1 to account for reflection of the transmitted light back into the laser rod, it should be noted that caustics are formed by the initial set of rays (before reflection) only. The multipass formula for intensity, which is believed to be a good approximation in general, is not used for investigation of intensity distribution near caustics.

WAVE THEORY OF THE CAUSTIC

The Diffraction Integral.

The geometrical optics (G.O.) theory identified the caustic as the locus of points (a,α) where $\partial\alpha/\partial\phi$ is zero, because this derivative appears in the denominator of the expression for the intensity. The wave theory works by expressing the field amplitude at a point in the region of the caustic in terms of a diffraction integral. The surface of integration is any surface over which the field is defined accurately by the G.O. theory. The surface chosen is the inside surface of the laser rod at radius r_1. The complex amplitudes at points (r_1,θ,z) on the surface are given by

$$(r_1,\theta,z) = [I(r_1,\theta,z)]^{\frac{1}{2}} e^{ikS'_2} \qquad (101)$$

wherein the units of A are such that the square of the magnitude gives

the intensity inside the medium of refractive index n_1. The optical path S'_2 from the source to the rod surface is given by

$$S'_2 \equiv S'_2(r_1,\theta,z) = \int nds = \sum_j n_j s_j \qquad (102)$$

evaluated along the ray AQ. The geometry is shown in Figure 19 where A denotes the point or line source, Q the point (r_1,θ,z) that generates the Huygens wavelet, and P the field point $(a,\alpha,0)$

The field at P is then

$$A(P) = (-in_1/\lambda) \int\int A(Q) \; e^{(ikn_1 - \sigma/2)S'_1} \; O(\theta,z)dq/S'_1 \qquad (103)$$

where dq is the area element at Q, S'_1 is the distance QP, and $O(\theta)$ is the obliquity factor for the Huygens wave source at Q:

$$O(\theta,z) = \tfrac{1}{2}(1 + \cos\varepsilon)\cos\beta_1 \qquad (104)$$

where $\varepsilon(\theta,z)$ is the angle between QP and the refracted G.O. ray at Q, and β_1 is the angle of refraction inside the medium n_1, i.e. the angle between the surface area element and the wavefront element.

Fig. 19 is projection on the transverse plane and thus does not show the vertical dimension z. If S'_1 is the transverse component of S'_1 . then

$$(S'_1)^2 = S_1^2 + z^2$$

and for the small range of z involved in the integration, the approximation

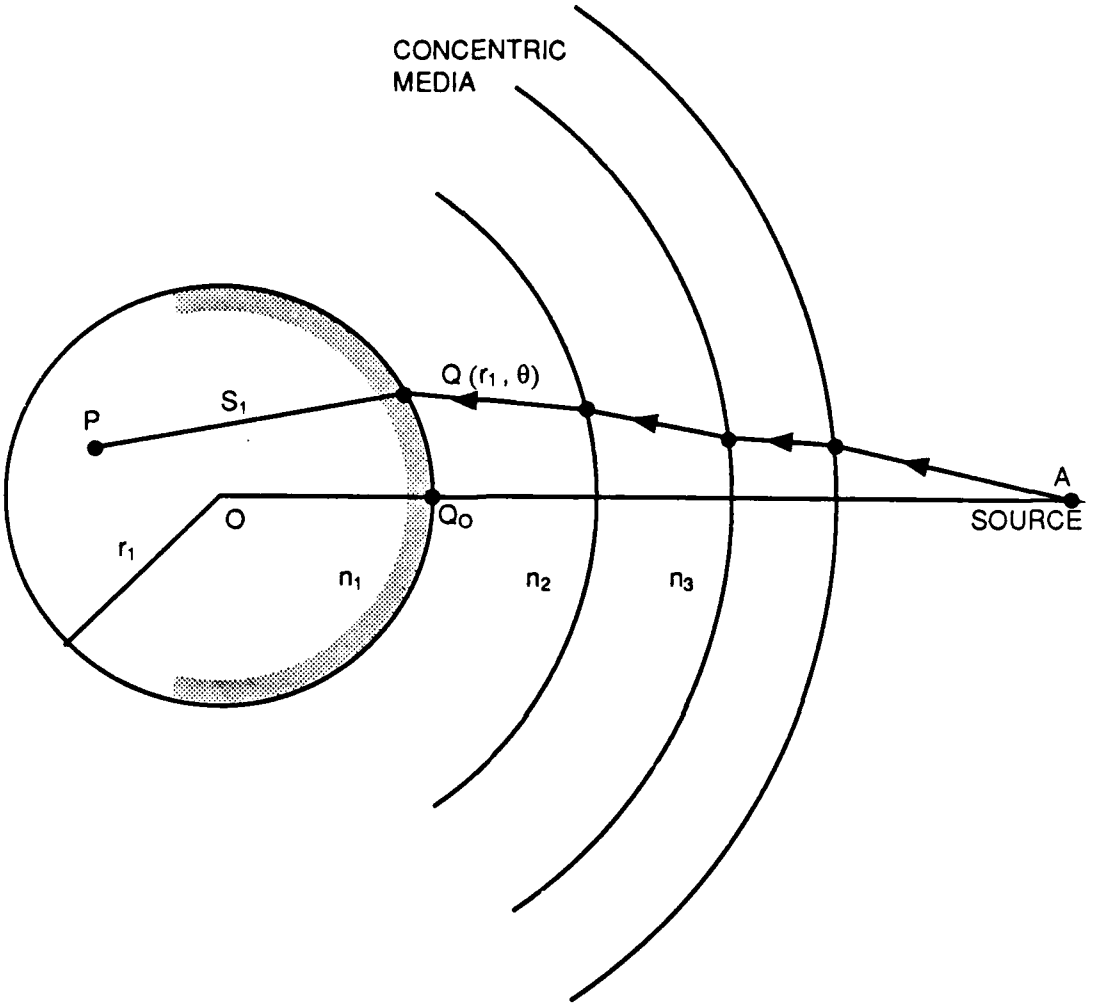

C88-8959

Figure 19. Projection of ray path on plane perpendicular to z-axis. The shaded area is the surface of integration used in the diffraction calculation. P is the field point, and A the source. The path from A to Q is determined by geometrical optics. QP is the line along which the Huygens wavelets propagate.

$$S_1' = S_1 + z^2/2S_1 \qquad (105a)$$

is made. Similarly

$$S_2' = S_2 + z^2/2L \qquad (105b)$$

where L has the dimension of length. The quantity L is infinite if A is a line source, i.e. A(Q) then has as its phase factor $\exp(ikS_2)$. Finally, with the area element expressed as

$$dq = r_1 d\theta\, dz$$

the diffraction integral becomes:

$$A(P) = (-in_1/\lambda)r_1 \int d\theta \cdot e^{ik(S_2 + n_1 S_1) - \sigma S_1/2} \; x$$

$$\int dz \cdot O(\theta,z)(S_1 + z^2/2S_1)^{-1}[I_1(r_1,\theta,z)]^{\frac{1}{2}} \exp[\{i \frac{k}{2}[\frac{n_1}{S_1} + \frac{1}{L}) - \frac{\sigma}{4S_1}\}z^2] \qquad (106)$$

The phase in the second integral is stationary at z = 0 and varies rapidly on either side of this point, so that this integral is approximated closely by the expression

$$Integal = [I_1(r_1,\theta,0)]^{\frac{1}{2}} O(\theta,0)/S_1) \int_{-\infty}^{\infty} e^{iK^2z^2} dz \qquad (107a)$$

and this last integral is equal to $(i\pi)^{\frac{1}{2}}/K$ where

$$K = K(\theta) = [(k/2)(n_1/S_1 + 1/L) + i\sigma/4S_1]^{\frac{1}{2}} \qquad (107b)$$

(The term proportional to σ is neglible compared to the term in k.) Because of this last expression one gets the $S_1^{\frac{1}{2}}$ *factor in the denominator of the θ integral in Eq. 106 for cylindrical waves, i.e. when 1/L is zero. At this point we specialize the calculation to this case and write for Eq. 107:*

$$Integral = [I_1(r_1,\theta,0)]^{\frac{1}{2}}\, O(\theta,0) \qquad (107c)$$

Substitution of Eq. 107 into Eq. 106 gives

$$A(P) = \frac{e^{3\pi i/4}\, r_1 n_1}{(n_1\lambda)^{\frac{1}{2}}} \int \frac{A(Q)\, e^{i\psi(\theta)} e^{-\sigma S_1/2}\, O(\theta,0)}{S_1^{\frac{1}{2}}}\, d\theta \qquad (108a)$$

for the field amplitude, and

$$I(P) = \frac{r_1^2 n_1}{\lambda} |J(P)|^2 \qquad (108b)$$

for the intensity, where J(P) is the integral in Eq. 108a. Note that in the expression for J(P) the amplitude $[I_1(r_1,\theta,0)]^{\frac{1}{2}}$ *has been written A(Q). The phase ψ(θ) is given by*

$$\psi(\theta)/k = S_2 + n_1 S_1 \qquad (109)$$

For large enough k the phase will change so rapidly as a function of θ (away from its stationary point) that again the stationary phase approximation can be used and the whole behaviour of I(P) is determined by the way that Ψ(θ) varies in form from one point P to another. In the case of practical interest here, k is not large enough for this approximation, but it is fruitful to investigate this asympotic form because it can give a quick approximation to the integral.

The ratio of intensities at two field points is the ratio of the corresponding quantities given by Eq. 108b and it is convenient to compare intensities to those on the axis of the rod where the G.O. theory gives an accurate estimate.

The Phase Factor.

The variation of Ψ/k with θ is shown graphically in Figure 20 for four field points, two in the illuminated zone, one on the G.O. caustic, and one in the G.O. shadow respectively, reading from top to bottom. (All the curves have a cut-off at the right hand end because of the critical ray.) The top curve has a minimum that identifies θ for the G.O. ray. The second curve has two points of stationary phase corresponding to the maximum and minimum, thus identifying two rays through the field point. One ray satisfies Fermat's principle with a minimum and the other satisfies it with a maximum. Interference occurs because of the two rays. Each of the curves can be represented by an equation that contains primarily linear and cubic terms when expanded about a θ-value of a little less than one radian. On the third curve, for a point located on the G.O. caustic, the linear term has zero coefficient. The bottom curve, which has linear and cubic terms of the same sign, has no extremum and therefore no G.O. ray.

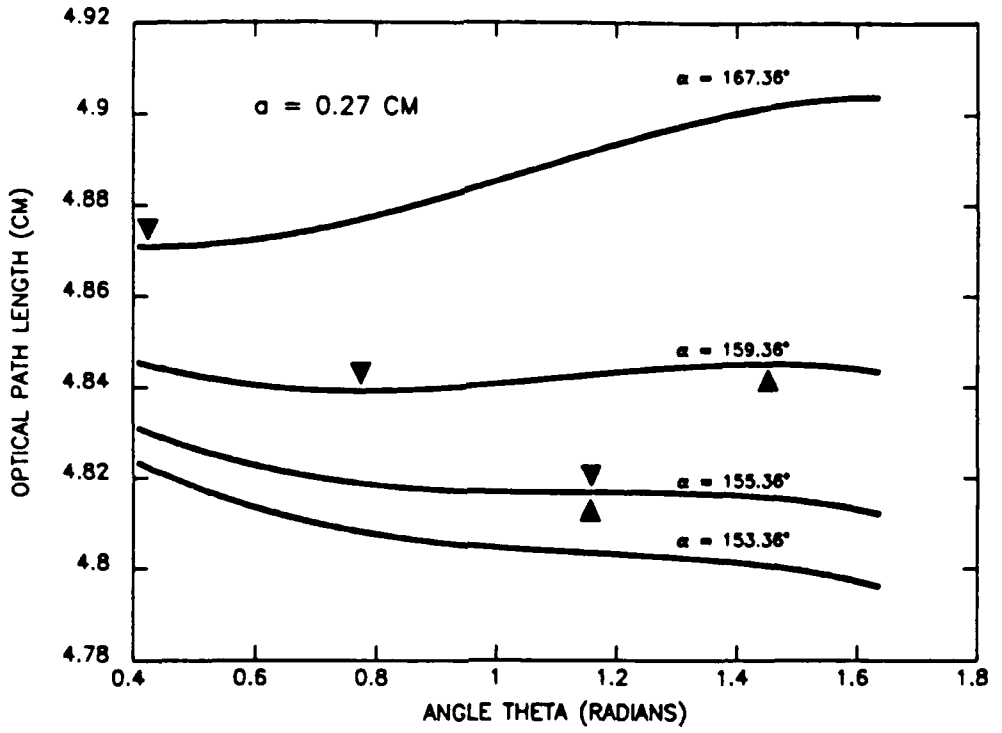

88-8960

Figure 20. Plot of optical path length defined by Eq. 109 versus θ, where S_1 is shown in Fig. 19 and S_2 is the optical path AQ. The geometry used in this illustration has four regions with radii 0.3275, 0.5, 0.65 and 4 cm and indexes of refraction 1.823, 1.333, 1.5 and 1. The solid triangles point to the extrema on the curves.

In the neighborhood of the caustic the field intensity will be greatest at the point for which the phase curve has the largest range of θ *that limits the range in* ψ *to approximately* π *. The phase will thus have the form of the second curve of Figure 20 with a vertical offset between maximum and minimum of somewhat less than* π *, and thus the corresponding point lies not exactly on the G.O. caustic but just inside the illuminated zone. This is analogous to finding that the maximum of the quantum mechanical wave function for a particle being turned on a potential slope occurs not at the classical turning point (where the wavefunction has an inflexion point) but on the downhill side of this point.*

If the amplitude of the Huygens wavelets were independent of θ *and the other factors in the integrand of Eq. 108a constant, the integrand would be of the form exp* $i(b\theta + a^3\theta^3)$ *which yields Airy functions (Bessel functions of order one-third) when integrated over a large number of cycles. The ratio b/a varies from one curve to the next in Fig. 20. In the shadow region were b has the same sign as a one would obtain the Bessel function* $K_{1/3}(y)$*, while in the illuminated zone where b/a is negative the combination* $J_{1/3}(y) + J_{-1/3}(y)$ *would occur. In each case the argument y is* $\{|2b/3a|(|b/3a|)^{\frac{1}{2}}\}$ *. The integral is readily obtained by combining Formulae 1 and 2 of I.S. Gradshteyn and I.M. Ryzhik "Table of Integrals, Series, and Products" section 3.695. (Academic Press 1980).*

Hence in the limit of large k the intensity at P as given by Eqs. 108 and the referenced formulae is

$$I(P) = (r_1^2 n_1/\lambda\, S_1) \cdot |4\pi^2 b/27a^3| \cdot \{J_{1/3}(y) + J_{-1/3}(y)\}^2 \cdot I(Q)\, e^{-\sigma S_1} x$$

$$< \cos^2 \beta_1(Q) > \qquad (110)$$

in the illuminated zone, with a similar formula having $\{K_{1/3}(y)\}$ for the shadow region. Here < . . > denotes an average value of the cosine-squared factor e.g. its value at a point midway between the maximum and minimum phase points.

Estimate of the Peak Intensity.

Although modern optics texts do not treat the subject of caustics it is no accident that the Airy function is tailored for their description. The Airy function is defined by

$$Ai(-x) = (1/3)\, x^{\frac{1}{2}} \{J_{1/3}(y) + J_{-1/3}(y)\} \qquad (111a)$$

and

$$Ai(x) = \pi^{-1}(x/3)^{\frac{1}{2}} K_{1/3}(y)\ , \qquad (111b)$$

where $y = (2/3)\, x^{3/2}$. (See M. Abramowitz and I.A. Stegun (Eds.) "Handbook of Mathematical Functions," pp. 446, 447, 478; especially Table 10.13.). It is not related to the Airy pattern $[J_1(x)]^2/x^2$ describing diffraction by a circular aperture.

The expression 111a will be used here, wherein y is $2(-b/3a)^{3/2}$, which is positive because b is positive and a negative in the region of interest. In terms of Eq. 111a,

$$\int_{-\infty}^{\infty} \exp i(a^3x^3 + bx)dx = (-2\pi/3^{1/3}a)\, Ai(b/3^{1/3}a) \qquad (112)$$

so that Eq. 110 now reads:

$$I(P) = (r_1^2 n_1/\lambda S_1)(4\pi^2/3^{2/3}a^2)[Ai(b/3^{1/3}a)]^2\, I(Q)\, e^{-\sigma S_1} \cos^2\beta_1(Q) \qquad (113)$$

The maximum value of Ai(-x) occurs at its first maximum, which is 0.53565666 at x = 1.01879297. Putting this value into Eq. 13 gives

$$I(P)\ (Maximum) = (5.4457/a^2)(r_1^2 n_1/\lambda S_1)\ I(Q)\ e^{-\sigma S_1} \cos^2\beta_1(Q) \qquad (114)$$

The specific curve of this type shown in Figure 20 that corresponds to $(-b/3^{1/3}a)$ being equal to x above has a vertical displacement between maximum and minimum ψ values (equal to $5(b/3a)^{3/2}$) of 1.7139 radians (98.2 degrees), thus putting the maximum just inside the illuminated region as expected.

This estimate of the maximum intensity expected in the caustic region has as its principal assumption the constancy of the intensity I(Q) on the inside surface of the rod over a region that takes in a large multiple of 2π in the phase function $\psi(\theta)$ on each side of its slowly varying part, i.e. that there be a large number of Fresnel zones on each side of the pair of G.O. rays. The assumption is not necessarily a good one in cases of practical interest. The various curves in Fig. 20 vary principally in their values of b. The coefficient a varies more slowly and the value to be used in Eq. 114 can be taken from the third curve i.e. the one with b equal to zero. The coefficient a^3 is determined from the table of values used to plot ψ/k .

Fig. 20 refers to points close to the caustic of Fig. 18 in the previous section "Transverse Pumping - Geometrical Theory." There, λ = 0.8 micron, a^3 = 3108, r_1 = .3175, n_1 = 1.823 and we get from Eq. 114

$$I(P)(Maximum) = 141.5\ I(Q)\ e^{-\sigma S_1} \cos^2\beta_1(Q)$$

For the other parameters applying to this particular configuration, including σ = 3 cm^{-1}, and β_1 = 40.57 deg. , the above relation becomes

$$I(P)\ (Max.) = 39.2\ I(0)$$

in terms of the intensity on the axis, for the caustic at radius 0.27 cm. As will be seen below this last expression over estimates the intensity by about a factor of 4.

Computation of the Integral.

A computer program was written by our subcontractor (Pharos Technical Enterprises) to calculate the intensity in caustics of the pump field on IBM PC computers and clones. The program is written in MicroSoft QuickBasic 4.00b and is called 8PGM2100.727. A stand-alone executable version is available which runs outside the QuickBasic environment, called PG88-007.EXE. The stand-alone version runs approximately twice as fast as the QuickBasic version. Either runs with or without an 8087 (or other) numeric coprocessor with no change in accuracy. Software emulation of the 8087's IEEE floating-point arithmetic format is done in the absence of the hardware numeric coprocessor, slowing the program by a factor of approximately 30.

The program calculates the Fresnel diffraction integral for two dimensional pumping geometries. The program does not (but could easily be modified to) dynamically adjust its step size. As a result it may be used only for problems closely approximating the case for which it was written. The program calculates the pump intensity at the field point (r,θ) within the laser rod for a single diode located at a radius approximately 6 times the radius of the cooling jacket away. The number of different media in the pump path is arbitrary; 4 were used in the test cases (air, water jacket, coolant, laser rod). The intensity is calculated for the first pass of the pump light through the rod. Similarly, it is assumed that pump fields from multiple diodes can be added using geometrical optics approximations.

The program divides the problem into 4 parts: data input, geometrical optics calculations, diffraction calculations, and data output.

Data input may be from a file or from the keyboard. The system may be edited and/or saved in a file for reuse. The program handles routine errors in file usage, such as specification of non-existant directory or file names.

The method of the program is to select a radius from the center of the rod through the diode. The far-field emission pattern of the diode is then projected from the diode, through the intervening media (if any), to the inner surface of the rod. The pump field is calculated at discrete, fixed-step intervals around the periphery of the rod. (This needs to be generalized to dynamically optimize the step size.) This step is called the geometrical factors calculation, and requires about 1 to 2 minutes for a 4 media geometry on a PC. It uses the G.O. theory of Section 1. The E field is presumed to be parallel to the axis of the system, which corresponds to the normal polarization of diode arrays oriented so that the long axis of the chips are parallel with the system axis.

The user may specify a range of field points, in either or both angle and radius, for the program to sept through automatically. For each field point the program integrates the contributions from all illuminated portions of the rod periphery, using linear interpolation between the points along the periphery. The use of linear interpolation increases the number of points along the periphery that must be calculated in the geometrical portion of the program, but minimizes the computation time in the diffraction portion of the program, striving for a good balance. The integration is done in fixed steps of angle around the rod; this needs to be generalized so that the program can optimize its computation time and handle a large range of cases. The diffraction

integral includes all the necessary terms to account for the cylindrical geometry, and includes the obliquity factor, which is a small (of order 10^{-6}) adjustment in the cases tested. It does not include a term to account for the fact that H vectors are not all parallel at the field point.

The data output is to the screen, to a printer (if specified), and to two disk files (if specified). Two output files are used to protect from data loss during unattended operation should a power failure occur during the short period that data are being written to a file.

In order to display the data, a group of complementary programs (8PGM0845.716, et al) were written in MathCad 2.06. They directly read the data files written by the diffraction integral program. MathCad provides a variety of tools for analyzing and plotting the data, and there seemed no need to provide an inadequate subset of its capabilities in the diffraction integral program. The files can also be read into other analysis and plotting programs, spread sheets, or word processor programs, if desired.

The diffraction integral program has been extensively cross checked against geometrical optics calculations, both outside of the rod and within the rod. The agreement has been found to be more than adequate, of the order of 10^{-4} or better for the cases tested. The penalty for this accuracy, and the lack of dynamic step-size adjustment is slower computation. The diffraction and output portions of the program require 3.5 to 7 minutes per field point on a PC/XT/AT class machine with a numeric coprocessor. The geometrical optics programs used for comparison were written by another programer, in a different version of BASIC (interpreted BASICA), utilize a different arithmetic (MicroSoft Binary Format instead of IEEE format), and run on a different machine.

Elsewhere in this report the geometrical propagation equations and the form of the Fresnel diffraction integral used are discussed. There are also displays of typical data including comparisons to the geometrical approximation.

Without the addition of dynamic step-size adjustment, the program is limited to applications in which the diode pump light illuminates approximately 180 degrees of the periphery of the rod, and the total pathlength difference from the diode to the rod surface between a ray propagating along the radius of the system and a ray propagating to the extremes of the rod (near where rays are reflected or refracted such that they miss the rod) is not more than about 4000 or 5000 wavelengths. The program presumes a Gaussian (in one dimension) far-field pattern from the diode.

Computational Example

The computation is illustrated for the following case:

$r_1 = 0.3175$ cm	$n_1 = 1.823$
$r_2 = 0.5$ cm	$n_2 = 1.333$
$r_3 = 0.65$ cm	$n_3 = 1.5$
$R = 4$ cm	$n = 1.$

The absorption coefficient in the rod is chosen to be $\sigma = 3\ cm^{-1}$, *and the refectivity at the wall is zero, because the caustic is a single pass phenomenon. The number of sources is chosen to be one, because each source produces its own pair of caustics. The source at R = 4 (on* $\theta = 0$) *produces the caustics running from roughly (0.235,± 140.85°) to the rod surface at (0.3175, ± 164.03°). About half-way along the caustic is the point (0.27, ± 155.36°) for which we made the rough estimate of the intensity using the Airy functions.*

The radii and refractive indices that we have chosen are not from a point design. They are chosen for purposes of illustration only. The radiation pattern from the source is characterized by the width ϕ_e equal to 6.436 degrees in the formula exp - $(\phi/\phi_e)^2$, since this particular value optimizes the flatness of the pump intensity distribution when multiple pump sources are used with a wall reflectivity of 0.97.

The amplitude and phase of the pump light just inside the surface of the rod on the side facing the pump source are readily tabluated as a function of θ using the two-dimensional G.O. theory, the phase being simply $2\pi/\lambda$ times the path length S_2; and it is adjusted to be zero at the entrance point on the central ray i.e. at Q_o in Figure 19. The path length $S_2(\theta)$ is as shown in Fig. 20 and the amplitude $A(Q)$ is shown in Fig. 21. The angle θ for the ray that passes through the caustic at radius 0.27 cm is 65.82 deg. (1.15 radians).

The range of θ in Eq. 108a is limited at ± 93.76 degrees where the angle of incidence β_1' at Q reaches 90 degrees. In the same equation, the obliquity factor has to take into account the fact that the surface on which the diffracting field is defined is not a wave front; and we do this by using the standard form $\frac{1}{2}(1 + \cos \varepsilon)$ for $O(\theta)$ and multiplying by $\cos \beta_1$ to convert the surface area element to the wavefront surface area, β_1 being the angle of refraction.

Figure 22a shows the intensity distribution along part of the circular arc a = 0.27 computed using Eq. 108, and that using the G.O. theory. The G.O. curve goes to infinity at about 155.36 deg., and elsewhere approximates the mean value about which the wave optics intensity oscillates. The peak intensity is 1.7634, which exceeds the G.O. value for the same point by 0.7776, and which is a factor 10.74 greater than the value on the axis. The increment 0.7776 thus deduced

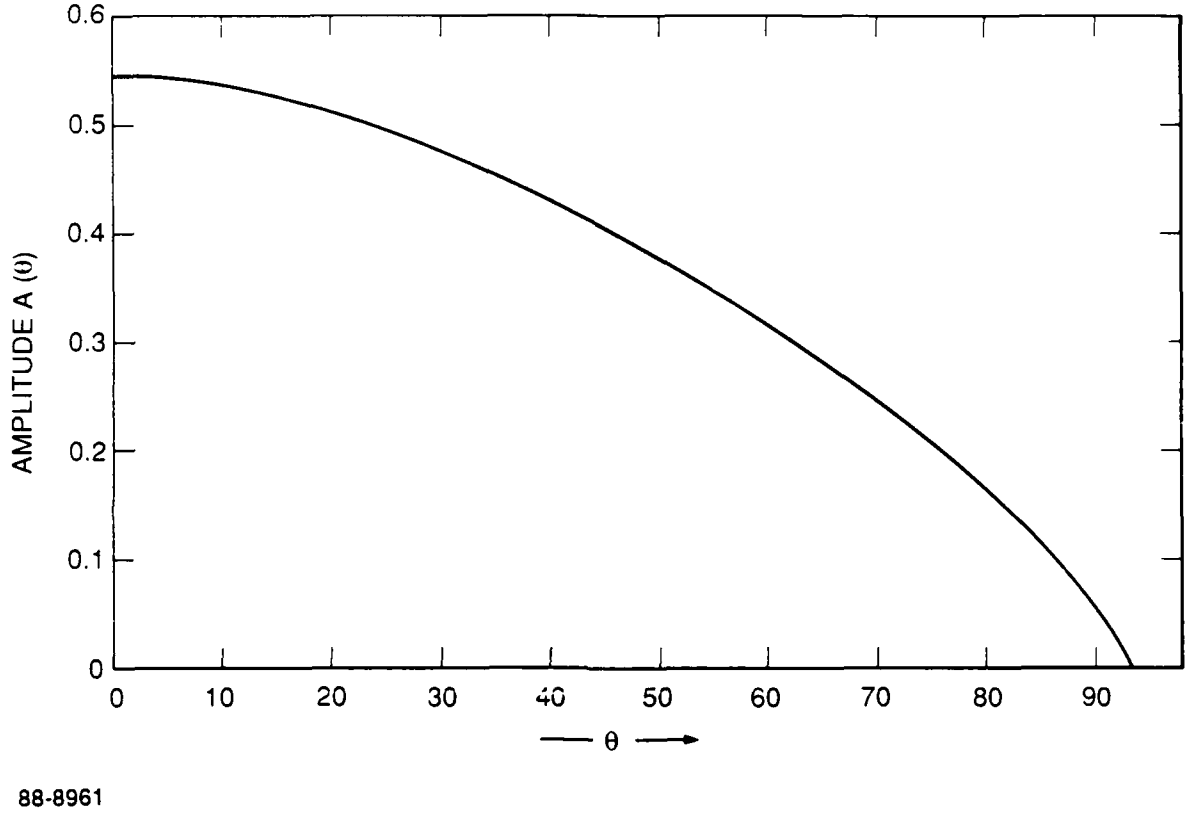

Figure 21. Plot of the amplitude of the source wave used in the diffraction integral, computed just inside the surface of the rod (radius 0.3175 cm), as a function of θ .

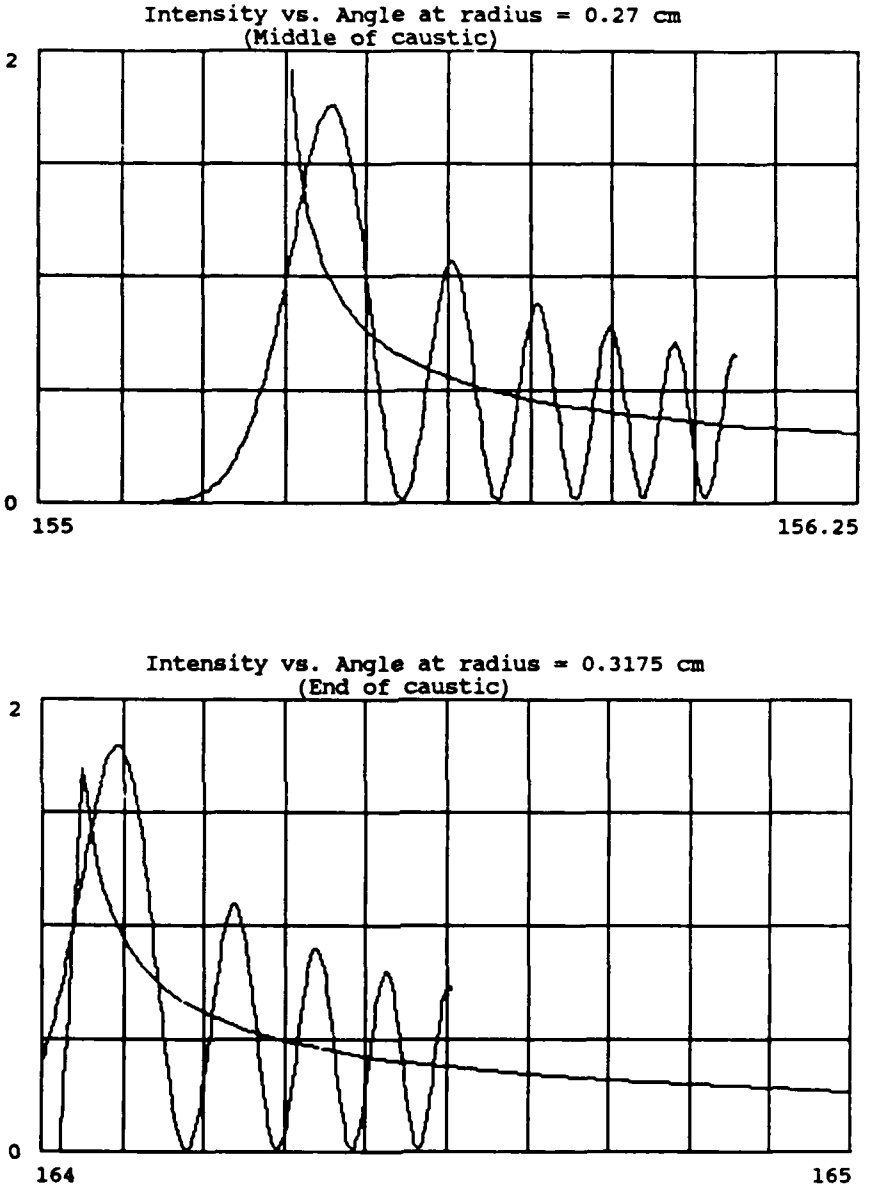

88-8962

Figure 22. G.O. and wave optics intensities computed along azimuthal cuts through the caustic at two radii. The computations use a single source, with zero reflectivity at the source radius, i.e. transmitted pump light is not returned to the rod.

for single pass (zero wall reflectivity) can now be added as a correction to the G.O. intensity due to one of the sources for multiple source illumination with any wall reflectivity. For example, with five equally spaced sources and wall reflectivity equal to 0.97, the G.O. illumination at the point (0.27, 155.445°) is 1.640 and at (0,0) is 0.9388. Adding the increment to the first number and dividing by the second gives a ratio of 2.58, compared to the 10.63 deduced for a single source, i.e. the intensity at this peak is 2.58 times the intensity on the axis of the rod. (Of course this result depends on the chosen pump absorption coefficient, in this case 3 cm^{-1}.)

The caustic intensity tends to increase towards the edge of the rod, this tendency being offset by the increased attenuation in the medium. Fig 22b illustrates the computation, again for a single pump source. For five sources, and wall relectivity of 0.97, the enhancement over the intensity on the axis at the caustic peak near the edge is a factor of 2.58.

With five equally spaced sources the caustics intersect in planes 72 degrees apart. There is a doubling of the excess intensity at these intersections. Fig. 23 shows a radial cut through one caustic. The excess over the G.O. intensity is doubled and added to the G.O. result, giving in this case an enhancement factor of 3.80 over the intensity on axis with wall reflec ivity 0.97.

The Realistic Case

Our model computations of caustic intensity reveal the expected fringes produced by interference between the two contributing optical paths The fringe spacing becomes smaller as one goes away from the G.O. caustic, as the angle between the contributing rays increases. Because the fringe spacing and the G.O. caustic location are both sensitive to the exact geometrical conditions the fringes in a real

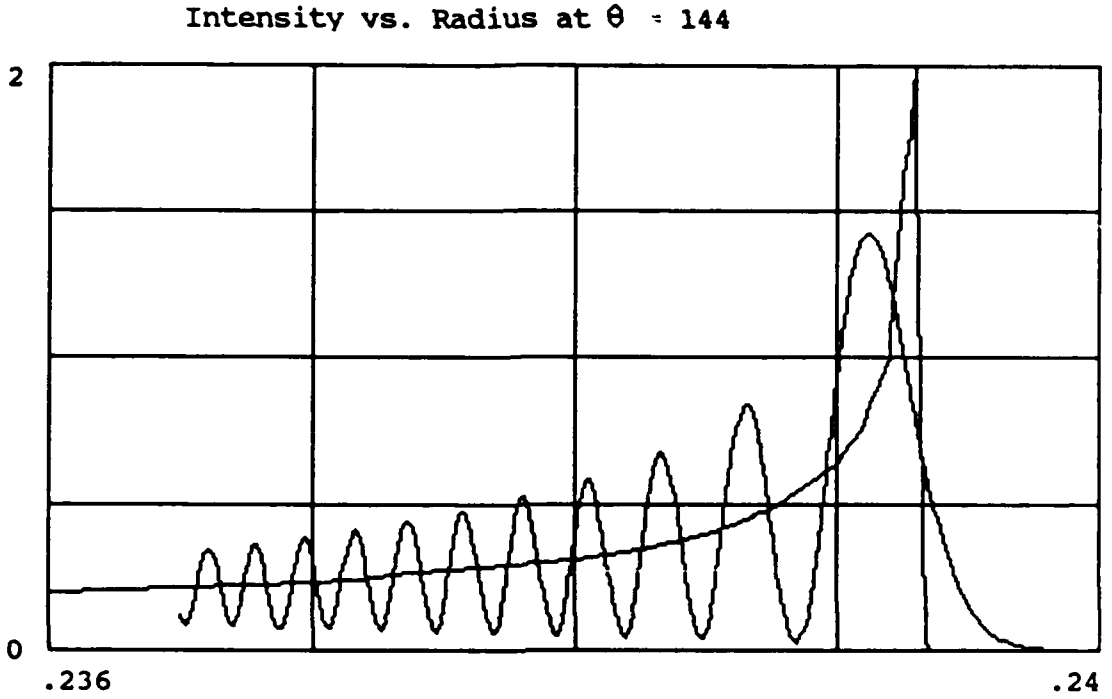

88-8963

Figure 23. Radial cut of intensity profile for a single source. The angle 144 degrees would be at a crossing of caustics from neighboring sources if five were used.

system will tend to become washed out. A principal contributing factor is the longitudinal propagation, i.e. the fact that the light through a field point originates from sources distributed along z emitting over a finite angular (δ) range.

The sensitivity of caustic location to the angle (δ) is readily demonstrated as follows. For the standard computational example that we have chosen above the angular location of the G.O. caustic at a = 0.27 cm is 155.362288 deg. This corresponds to transverse propagation, $\delta = 0$. When δ has some other value, e.g. 1 deg., the refractive indices (1.823, 1.333, 1.5, 1) are replaced according to Eq. 43 by a new set (1.823194, 1.333089, 1.500127, 1); and with these new parameters the angular position of the G.O. caustic changes to 155.369126 deg. For 1 deg. steps in δ up to 10 deg. the angular position of the caustic α_c at radius 0.27 cm is found to satisfy the following quadratic expression in δ :

$$\alpha_c = \alpha_c(o) + 0.006853\delta^2$$

where δ is in degrees. For example δ = 3.82 deg. will move the caustic at a = 0.27 through 0.10 deg. which is the displacement from the principal maximum to the first minimum. Thus δ ranges of a few degrees are sufficient to wash the fringes out, producing an intensity that closely matches the value predicted by G.O.

The important problem is the estimation of the peak intensity. The Airy function calculation that produced Eq. 114 overestimated the peak; so that method is unsuitable. The theory assumed a uniform amplitude distribution at the surface of the rod, instead of the actual distribution shown in Fig. 21. Replacing the distribution by a linear one corresponding to the tangent to the amplitude curve will also give a closed form mathematical expression for the intensity, but computational effort is still needed to get the a and b values in the phase

expression. (See Eq. 112.) It is easier to run PTE's program for the integral at a few points on a line that intersects the caustic, and get the intensity on the first peak.

Figs. 22 and 23 show that the peak intensity is of the order of 1.5 to 2 times the G.O. value at the same point. Thus the problem reduces to determining the distance from the G.O. caustic (which occurs at the inflection point on the Airy Function type curve) to the first peak. Again this would seem to require determining the position dependence of the phase coefficients a and b. We know of no short cut, like determining a Fresnel number for example, that will tell use the position at which to compute the G.O. intensity. (The Fresnel number comes out of a quadratic phase dependence rather than a cubic one.)